DTC Testing and Evaluation Annual Report

Build operational storm-scale data assimilation testing system and test DA advancement for convection forecast

July 2018

Data Assimilation Team

Table of Content

1. Introduction

High-Resolution Rapid Refresh (HRRR) is a key component of the NCEP operational modeling suite to provide high-resolution storm-scale model forecast. The HRRR system is not only used as the backbone of accurate short-range severe weather, aviation, and energy forecasting, but its model physics and data assimilation configurations will also be used as a reference to build the next generation FV3-based operational storm-scale modeling system. A functionally similar testing system to operational HRRR that is available for the use by the research community is a critical link to encouraging the broader storm-scale modeling community to make their research available to operations. The DTC built and maintains such an HRRR system on NCAR's supercomputer and makes this system available to the research community. The DTC DA team also acts as the first user of this system by conducting a series of operational-needs-based experiments to ensure the robustness of the functionally similar operational environment for testing the HRRR system. These exercises with the HRRR system will also help the DTC DA team build critical expertise in storm-scale data assimilation to provide high quality support to the community users of the HRRR testing system. In AOP 2018, the testing and evaluation (T&E) focus of the DTC DA team is exercising new DA techniques for radar data assimilation as there are many active research community developments in this area.

During AOP 2017, a series of experiments were conducted to test the impact of assimilating radar radial velocity on the HRRR forecast. In this work, the DTC DA team used the same infrastructure to extend the T&E to test the impact of dual-polarized quality controlled (DPQC) radar radial velocity data on HRRR forecast. The DPQC radial velocity is expected to keep most of the observed radial velocity from the US operational radar network after quality control with dual-polarized information to remove non-meteorological radial observations. Unlike over-quality controlled NCEP BUFR radial velocity data, these new data should lead to better storm detection and forecasts with proper data assimilation techniques.

The DTC processed those new DPQC radial velocity data by "bufrizing" them and dealiasing, studied how to effectively implement the new data using GSI through single cases, and conducted several week-long retrospective experiments to evaluate the impact of the new dataset on improving the convective forecast within HRRR. The results from those experiments will serve as references for selecting the optimal configuration for the future HRRR operations.

2. Data Pre-Process

The DPQC radial velocity data are provided by the NOAA National Severe Storms Laboratory (NSSL) in the form of single tilt observations saved as NetCDF files under individual folders for each radar. The data format GSI can use is a single BUFR file including all observations within a certain time window from all radar stations. Therefore, the DTC DA group developed a system to "bufrize" the data, which includes:

- A Fortran program to read in a tilt of radial wind observation from a NetCDF file, find the tilts from the same volume scan and assign the correct Volume ID, scan ID and VCP type, and then write all observations into a single BUFR file that GSI can read and use.
- The scripts generate the list of NetCDF files that include radial wind observations within a time window for all radar stations in the testing domain. This file list is used by the above Fortran code to generate a BUFR file used for the GSI analysis.

One week of DPQC radial velocity data were processed using this system to generate hourly radial wind BUFR files for retrospective experiments.

In radar observations, radial velocity is aliased when the true radial velocity is larger than the unambiguous velocity of a radar or Nyquist velocity. Radial velocity observations need to be de-aliased before the data can be used in the analysis. Because the DPQC data have not been de-aliased, a dealiasing program had to be developed before applying those data in the HRRR GSI analysis.

DTC DA group studied different dealiasing techniques. There are two groups of dealiasing algorithms: the continuity check and the reference check. We decided to develop a dealiasing program with three steps in a reference check:

The true velocity (U) is related to the observed velocity (V) as follows:

$$U = V + \kappa V_0 \qquad \kappa = \pm 0,\ \pm 1,\ \pm 2,\ \ldots$$

where V is the observed radial velocity that may be aliased, and U is the velocity after dealiasing. $V_0 = 2v_a$ is the ambiguous velocity interval, and κ is the integer multiplier needed to remove Nyquist aliasing ambiguities from V. κ is determined by the difference between the measured radial velocity and a reference radial velocity at the same radar measured point. The accuracy of the reference radial velocity is the key to the success of the dealiasing process and it can be obtained from three resources, as discussed below.

Resource 1. From model forecasts (Global dealiasing)

Because a high-resolution model forecast, such as from HRRR, can represent the wind environment with good quality and over the whole observation domain, using model forecasted radial velocity as a reference is the easiest way of obtaining the reference wind. The model forecast is independent from the observations and carries information from different observations nearby as well as other observation types. Hence the reference radial wind is the most efficient resource to de-alias the real observations. We performed tests to find out what is the best forecast length of HRRR forecast to be used as the reference and found 1-h to 3-h work well for this purpose. So, in our data process, the 1-h HRRR forecast, valid at the same time of the observation BUFR file cycle, is used.

Resource 2. From local average of the radial velocity (Local dealiasing)

Another way to obtain reference radial velocity is to calculate an average radial velocity using the observed radial velocities within a specified geometrical window for each observation point. This locally generated reference wind is calculated after the global dealiasing because it can only handle a small area when dealiasing. Local dealiasing is performed based on the same concept as the global dealiasing, but using a different reference wind.

Resource 3. From VAD (VAD dealiasing)

A third way to obtain a reference radial velocity is to generate Velocity Azimuth Display (VAD) wind, first based on whole radar volume observations, and then interpolate VAD wind to each radial wind observation location to serve as the reference. Unlike the local reference method, VAD wind is a representation of environment wind but can be too smooth and therefore miss local information that is critical for the successful dealiasing.

The dealiasing program we developed generates all three reference radial winds and applies them to the observed radial velocity in the order of global, local, then VAD dealiasing. Figures 2.1, 2.2, and 2.3 are examples of dealiasing for three elevation angles from a radar station at Paducah, KY (KPAH).

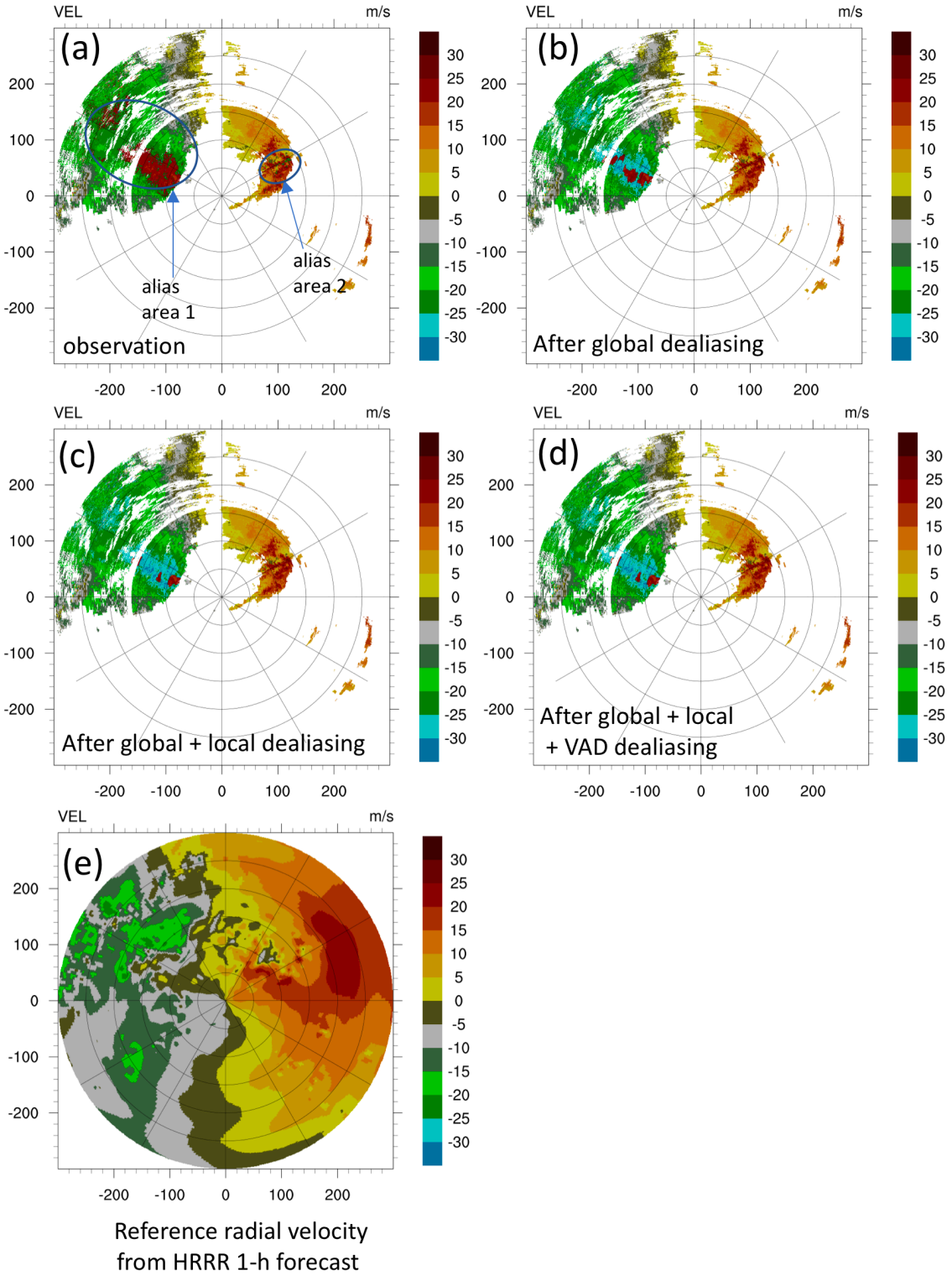

Figure 2.1, Dealiasing of radial velocity: The tilt is a 0.5-degree elevation angle from radar KPAH.

In radar observations at elevation 0.5 degree (Fig 2.1a), there are mainly two areas showing the aliased RW observations: a large aliased RW area (area 1) in radial wind toward the radar (negative velocity) and several aliased RW sparks (area 2) within radial wind away from the radar (positive velocity).

After global dealiasing (Fig 2.1b), most of the aliased RW in area 1 have been corrected, with some still aliased in the area near the radar location. Global dealiasing also helped area 2 but still left a few aliased spots. The key to get successful dealiasing is the quality of the reference radial wind. From the plot of background radial wind (Fig. 2.1e), we can see the areas difficult to correct are the areas where the HRRR forecast gave small radial wind speeds, which does not match the expectations from wind observations. Because the most coverage of the 0.5-degree elevation scan is within the PBL level, especially observations close to the radar station, the wind forecast from HRRR in those areas can have large forecast errors, which will certainly impact the correction when dealiasing.

Local dealiasing (Fig. 2.1c) helped aliased area 1 and further corrected some aliased RW left by global dealiasing, but still there are small areas of aliased RW left in area 1. It is hard to find the difference after local dealiasing in area 2.

VAD dealiasing (Fig.2.1d) didn't remove the aliased RW left from global and local dealiasing.

Figure 2.2 is similar to Figure 2.1 but with elevation angle 0.9 degrees. The same two major areas in the observation show the aliased RW (Fig. 2.2a). The aliasing in area 2 in the positive RW area becomes much larger. When the elevation angle increases, the coverage area also increases and the quality of the reference wind from the HRRR forecast has improved (Fig. 2.2e). We can see that global dealiasing did a much better job in both aliased areas. All aliased RW in area 2 have been corrected and only a small portion of the RW are still aliased in area 1 (Fig. 2.2b). At this elevation, local dealiasing (Fig. 2.2c) successfully corrected the remaining portion of the aliased RW after global dealiasing. The VAD dealiasing step (Fig. 2.2d) gave the same results as after local dealiasing.

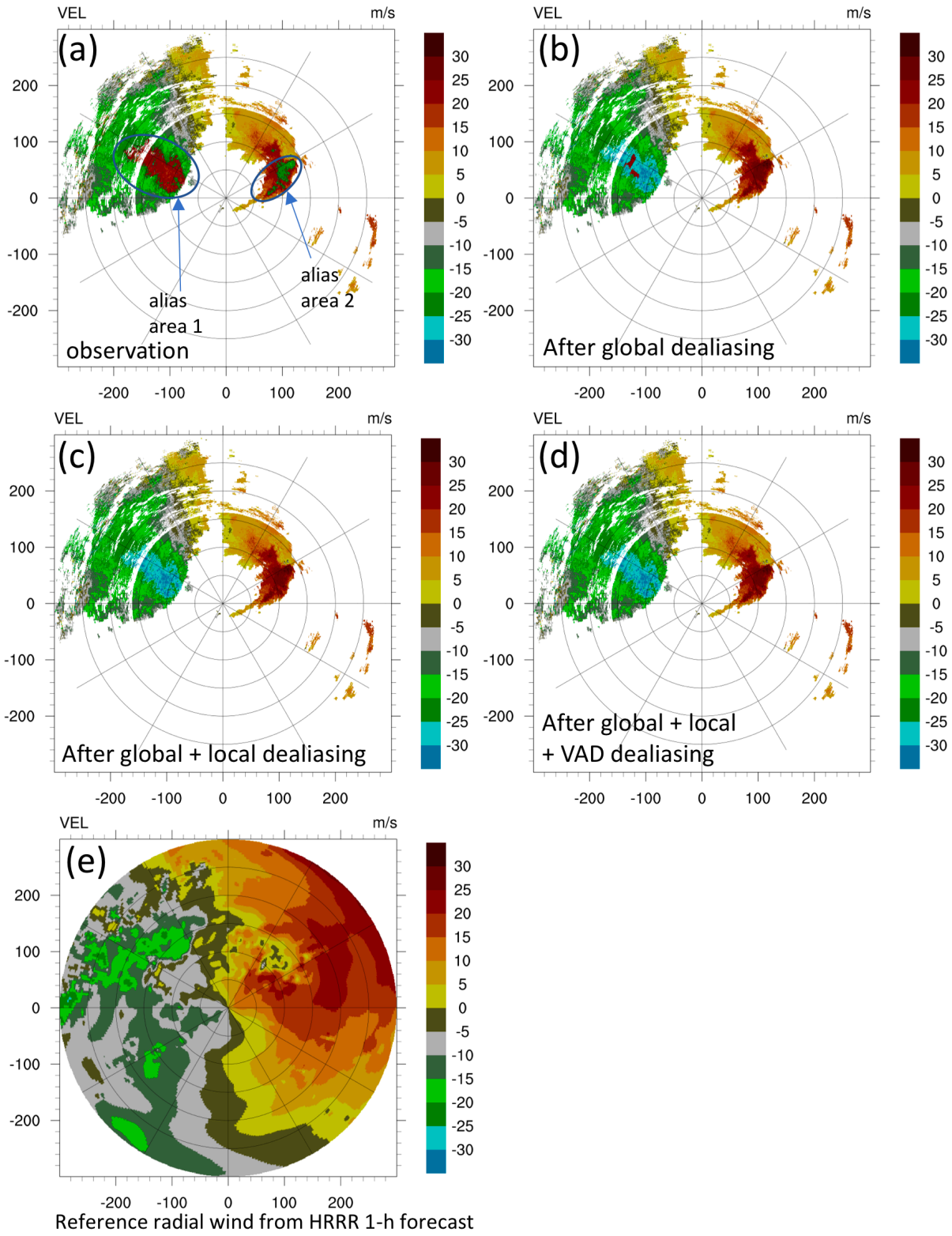

Figure 2.2, Dealiasing of radial velocity: The tilt is 0.9-degree elevation angle from radar KPAH.

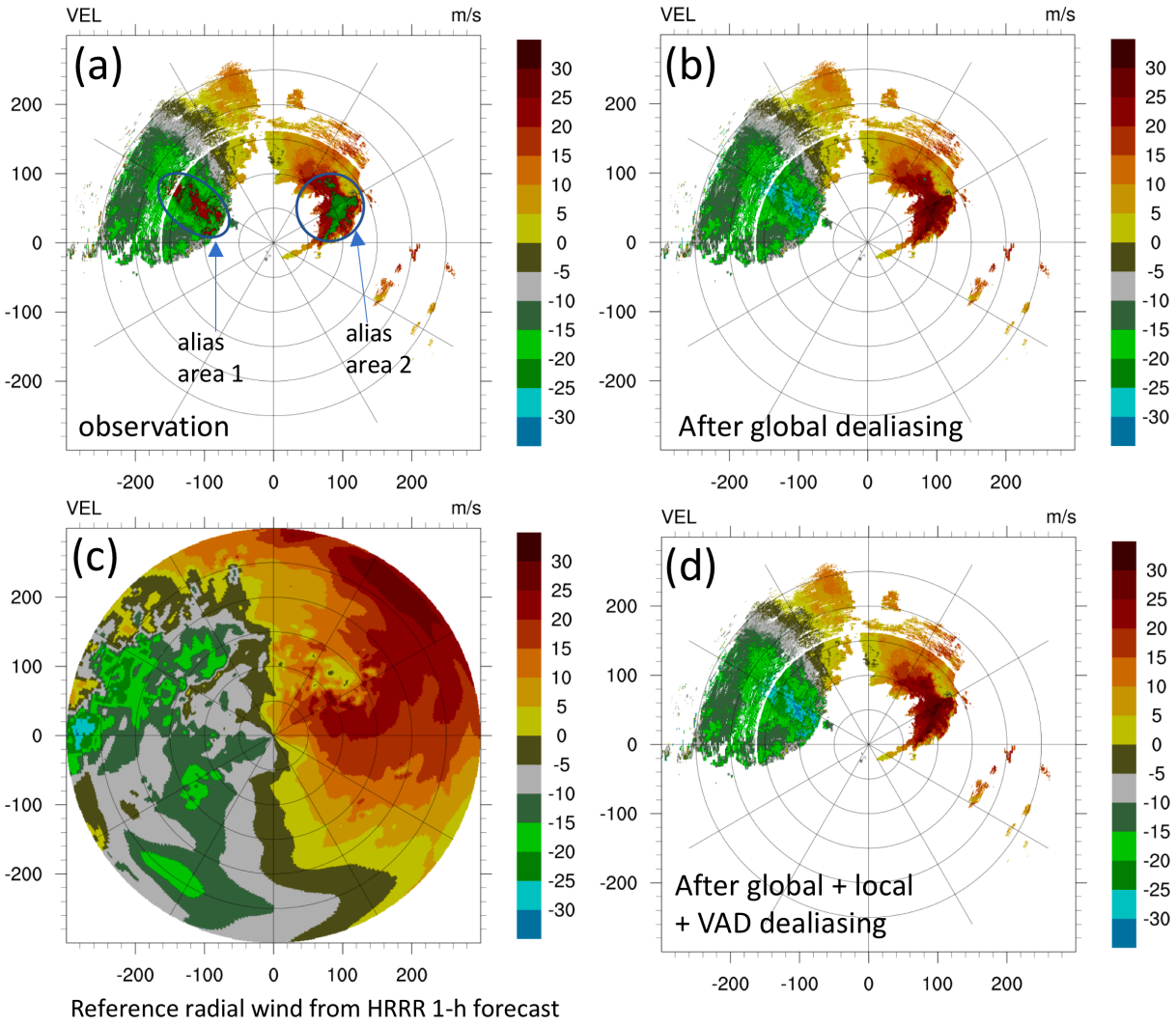

Figure 2.3, Dealiasing of radial velocity: The tilt is 1.3-degree elevation angle from radar KPAH.

Figure 2.3 is the same as figure 2.2 but for elevation angle 1.3, though we are not showing individual figures for local dealiasing after global dealiasing. This figure is shown to further confirm that the dealiasing program developed by the DTC DA team can remove all the aliased RW for elevation angles higher than 0.5 degrees.

For the 0.5-degree elevation scan, our program cannot correct all the aliased RW, so we tossed out the 0.5-degree elevation scan observations in our data process for the retrospective experiments.

3. Single case study to understand the data and RW analysis schemes

Before running expensive week-long retrospective experiments to study the impact of the new DPQC radial velocity on the HRRR forecast, a series of standalone GSI runs from the 00Z HRRR cycle on June 27, 2018 were conducted with different configurations to study the following:

- The characteristics of the GSI radial velocity observation operator.
- The effect of VAD quality control on the radial velocity.
- The difference in analysis using NCEP BUFR radial velocity data, which is the operational data feed for RAP/HRRR analysis, and DPQC radial velocity observations, which are from NSSL and have been "bufrized" and dealiased by the DTC.

3.1 Default and modified radial velocity observation operator in GSI

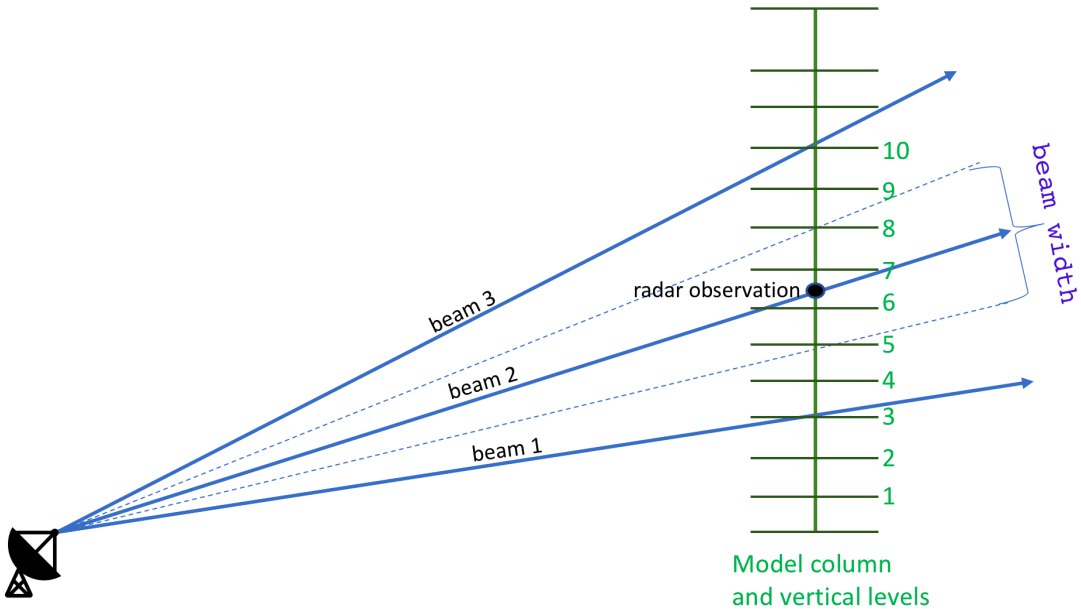

Figure 3.1, Schematic plot of radar observation beam and beam width, and the model levels within the beam width.

After studying the GSI radial velocity observation operator, we noticed the current scheme may miss some radial velocity information when applied to a high-resolution model. The current radial observation operator is calculated as following:

- Find the beam width around a certain observation and the model levels within this beam. In this schematic plot (Figure 3.1), levels 5, 6, 7, and 8 are within this radar radial observation beam.
- Calculate radial velocity from the background for levels 5, 6, 7, and 8. Find the maximum and minimum background RW.

- Compare the radar radial velocity observation with the maximum and minimum of the background radial velocity from the levels within the beam width, and decide the final background radial velocity for this observation point as follows:
    - If the observation is larger than the maximum background RW, use maximum background RW as final background RW.
    - If the observation is smaller than the minimum background RW, use minimum background RW as final background RW.
    - If the observation is between the maximum and minimum background RW, use observation values as final background RW.

This radial velocity observation operator will minimize the innovation of radial velocity and thus minimize the impact of the radial velocity. This operator is good for a background that has the maximum and minimum background velocity close to each other. But when we have high resolution models like HRRR, which can produce large vertical shear, ending up with big gaps between the maximum and minimum background radial velocity within the beam width, the innovation from this operator can have too many 0 innovations that miss useful storm scale wind information. So, we modified the RW observation operator to use the background radial velocity calculated at the observation point to calculate the innovation.

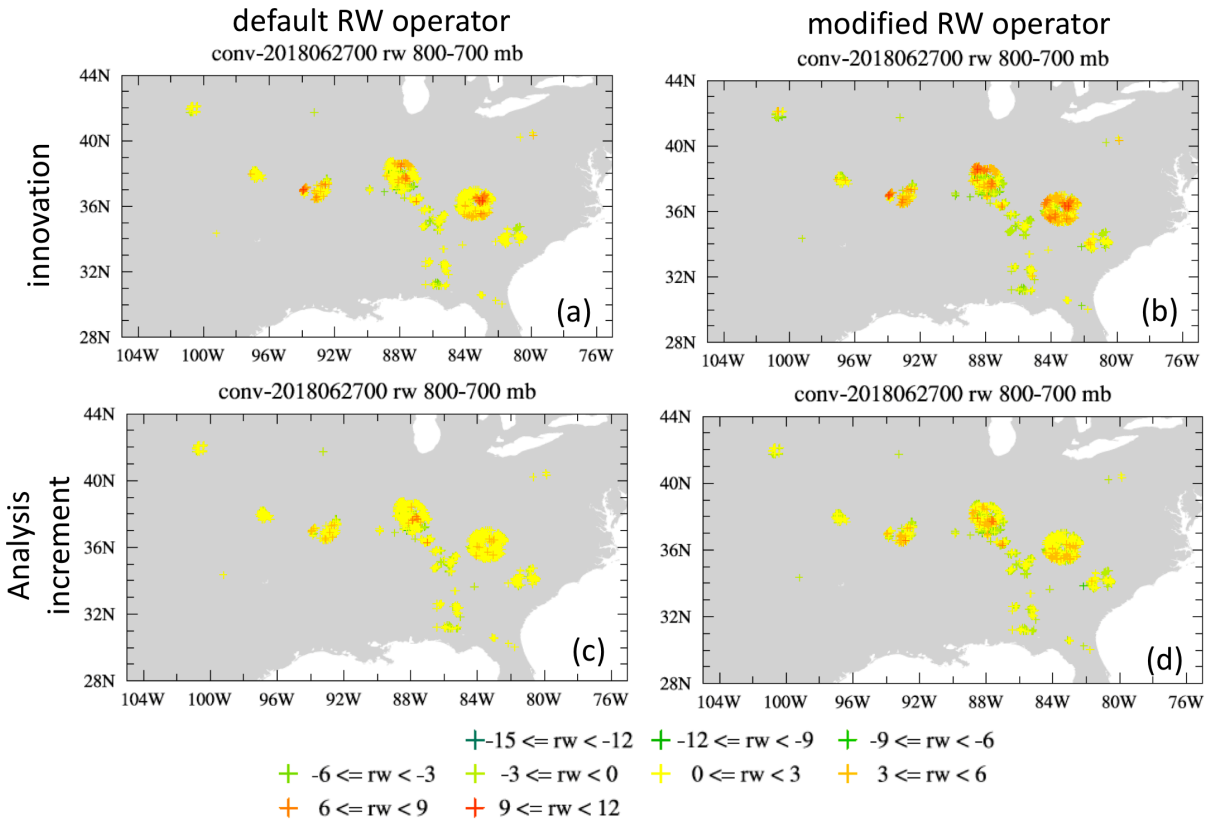

Figure 3.2, Radial velocity innovation (upper row) and O-A (lower row) in radial velocity observation locations between the 800-700 mb levels from GSI analyses with the default RW operator (left column) and modified RW operator (right column).

Figure 3.2 shows both innovations and analysis increments (O-A) of radial velocity from the default RW operator and the modified RW operator. We can see in Fig 3.2b that the modified RW operator brings in more innovations, compared to the default operator as shown in Fig 3.2a. These differences due to the RW operator can also be seen in the analysis increments (Fig. 3.2d). By using the modified operator, the analyzed radial velocity has bigger O-A compared to the results when using the default observation operator (Fig 3.2c).

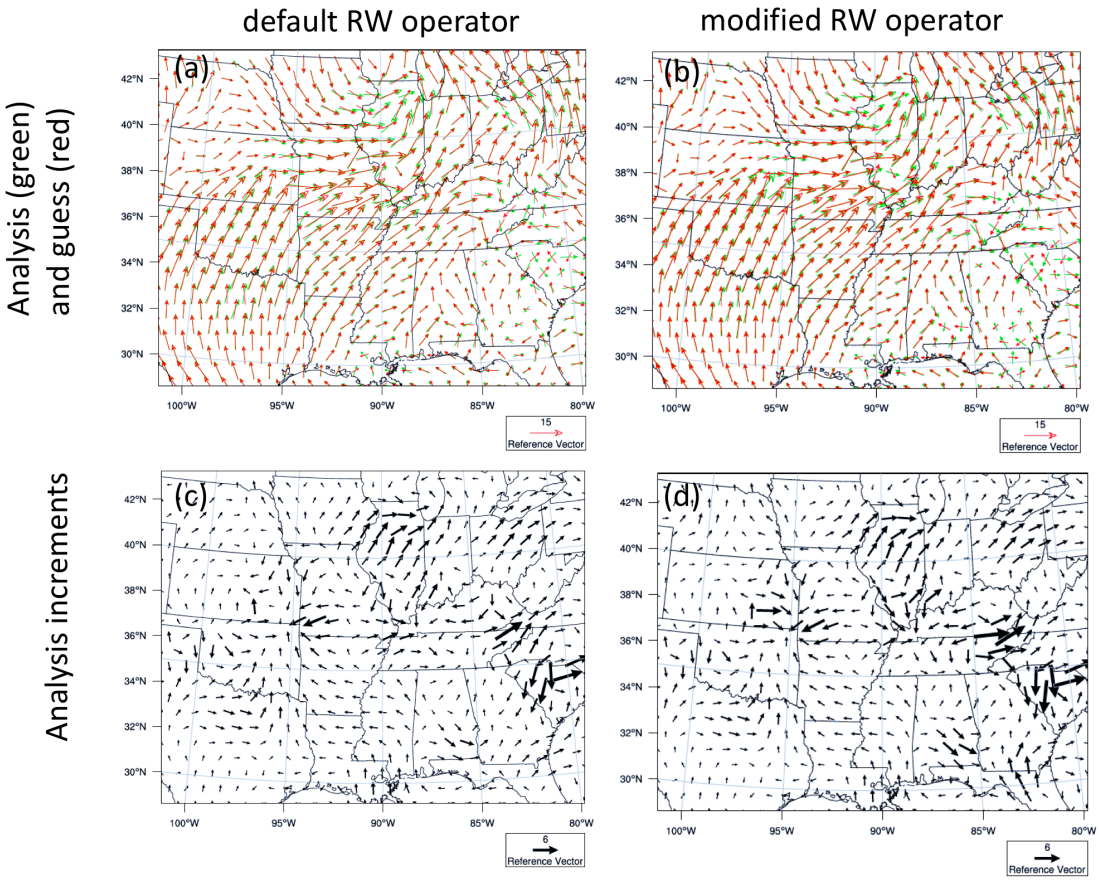

Figure 3.3, Background (red) and analyzed (green) wind vector (upper row) and wind analysis increments (lower row) at model level 7 from GSI analysis using the default RW operator and the modified RW operator.

Figure 3.3 examines the difference between the two radial velocity operator schemes through a wind vector field. It is hard to find the difference in full wind vector analysis fields (Fig. 3.3a and b), but the differences are very clear in the analysis increment wind vector fields (Fig. 3.3c and d). The modified operator shows more large vectors in many radar observation regions.

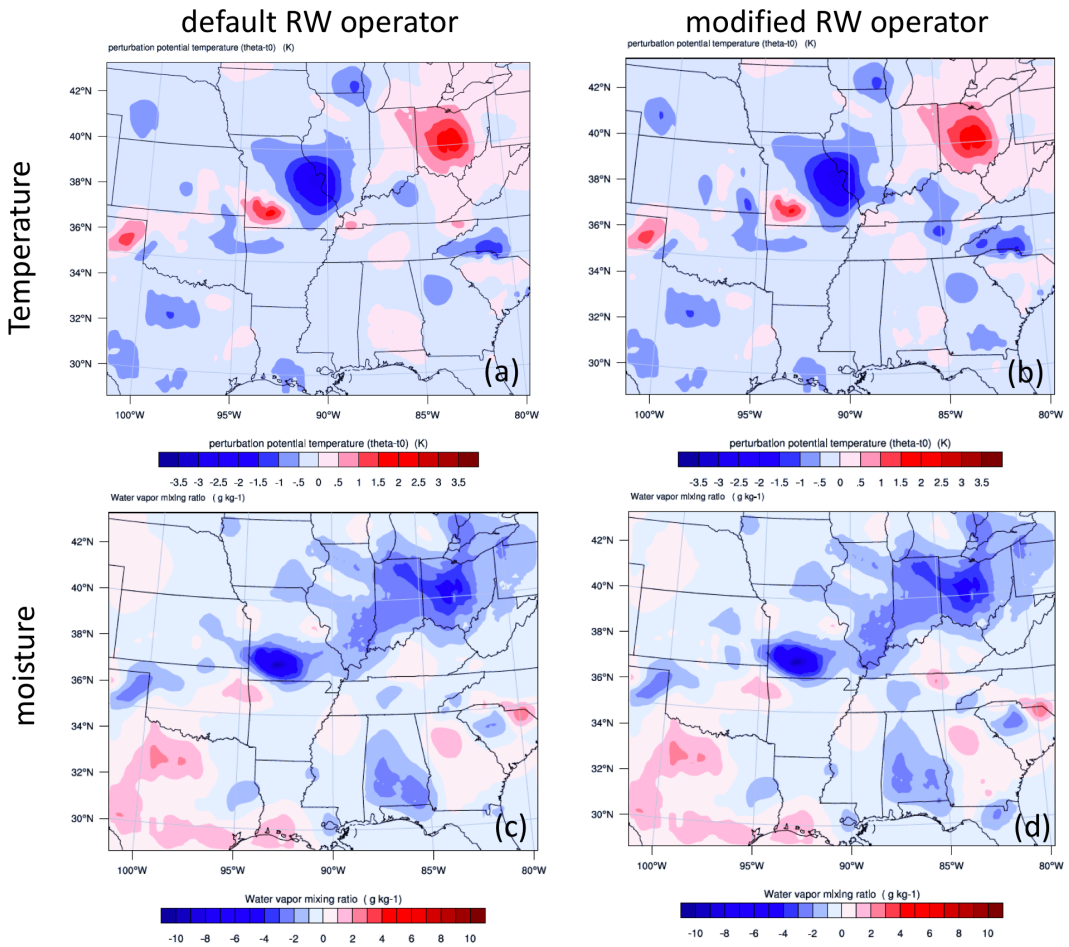

Figure 3.4, Analysis increment at model level 7 for temperature and moisture for the default and modified operators.

Figure 3.4 shows the temperature and moisture analysis increments from the radial velocity analysis, which was mainly induced by wind-mass balance and moisture analysis variable definition. We can see that the overall patterns of the temperature and moisture analysis increments are very similar between the two radial velocity operators. Still, we think the modified operator should be more suitable for GSI analysis with storm scale models.

3.2 Impact of VAD quality control on GSI radial velocity analysis

When GSI reads in the radial velocity observations, it has an option to use VAD wind to conduct quality checks for each individual radial velocity observation. In our test, we found this VAD wind QC is so strict that most of the radial velocity observations end up being rejected. In our test case, about 2,000 radial velocity observations were used in the analysis with VAD QC, but the number of radial velocities used in the analysis increased to 20,000 when VAD QC was turned off. So, VAD QC tossed around 90% of the radial velocity observations. This strict VAD

QC may be one of the reasons that our previous radial velocity impact experiments with HRRR generated neutral results.

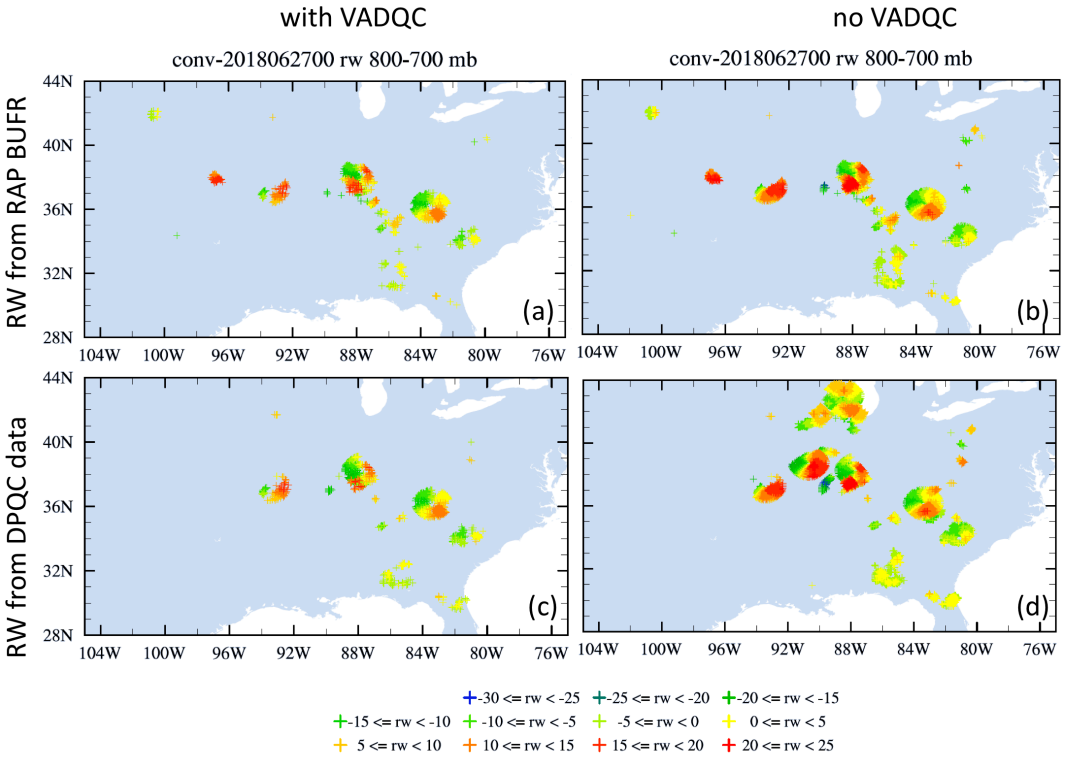

Figure 3.5, The distribution of radial velocity observations used in the GSI analysis, including radial velocities from the NCEP BUFR file (upper row) and the DPQC radial velocity file (lower row), and analysis with (left column) and without VAD QC (right column).

Figure 3.5 illustrates the distribution of the radial velocities that are used in the analysis within the 800-700 mb layer. It is clear that many more observations are used when VADQC is turned off. Interestingly, with VAD QC applied, the analysis using the DPQC radial velocity file (Fig 3.5c) has fewer observations used than the analysis with NCEP BUFR file (Fig 3.5a), while we were expecting DPQC to include more radial velocity observations because of the self-controlled dealiasing process. After turning off the VADQC, the analysis with DPQC radial velocities does seem to use more radial velocity observations, with many new radial velocities from radar stations located west of Lake Michigan (Figure 3.5d). Comparing with Fig. 3.5b, turning off VAD QC in GSI analysis using the NCEP BUFR file does add on many new observations, but those new observations are mostly from radar stations already used in the GSI analysis with VADQC turned on. The reason for VADQC having a different impact on the BUFR and DPQC data is because the VAD data used in the QC were generated based on the same data source that generated NCEP BUFR file. So, there are matching VAD observations with the BUFR radial velocity observations. However, the DPQC RW were collected from NSSL and includes several new radar stations, which have no matching VAD observations. This mismatch of VAD observations and radar stations lead to a rejection of all observations from stations that have no VAD observation

available. So, the GSI analysis with VADQC and DPQC data end up with even fewer observations used. VADQC has a bigger impact on DPQC observations because of missing VAD observations for some radar stations.

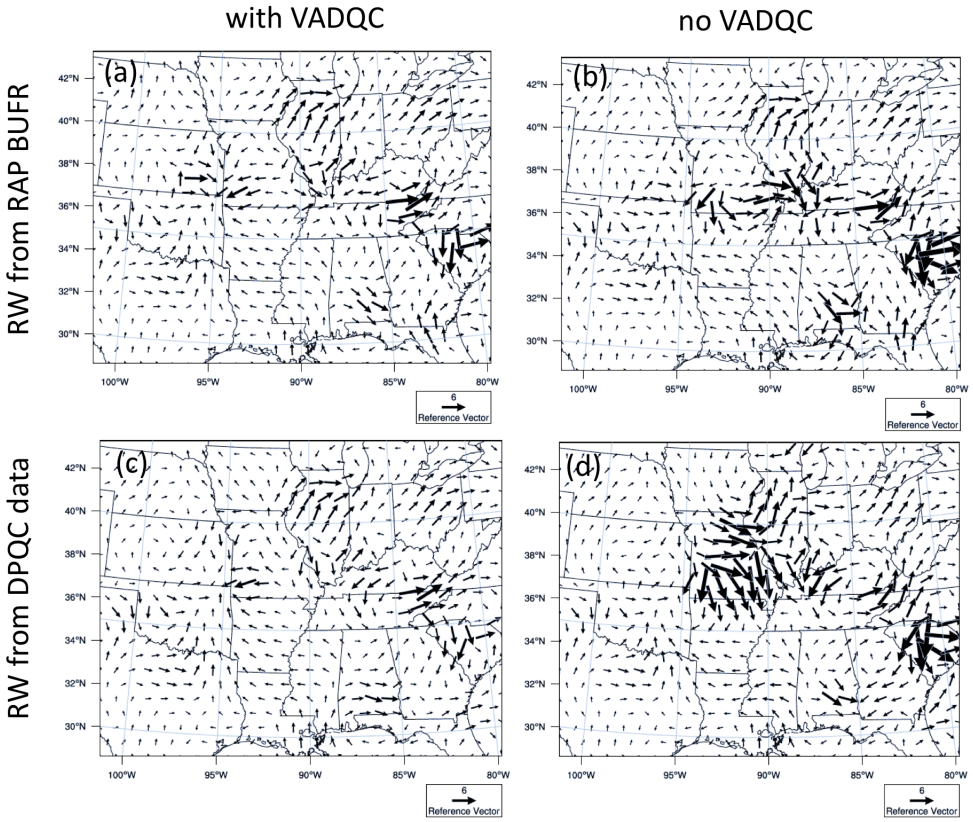

Figure 3.6, Wind analysis increments at model level 7 from GSI analysis using NCEP BUFR file (upper row) and DPQC radial velocity (lower row), and with VADQC (left column) and without VADQC (right column).

To further confirm our conclusions about VADQC, we also plot in Figure 3.6 the wind increments. The same characteristics were found that VADQC tossed lots of radial observations, even more so for the analysis using DPQC radial velocity (Fig 3.6c). After turning off the VADQC, many more radial velocities showed up and made for larger impacts in the GSI analysis, especially with the DPQC radial velocity observations (Fig 3.6d).

3.3. Comparing BUFR and DPQC radial velocity data

After studying the radial velocity observation operator and VAD quality control in GSI analysis, we decided to use the modified radial velocity observation operator, which uses the radial velocity calculated from background wind at the observation location as the final background radial velocity, and turned off the VADQC in a single case study to compare the impact of the radial velocity from NCEP BUFR file and DPQC data processed by DTC.

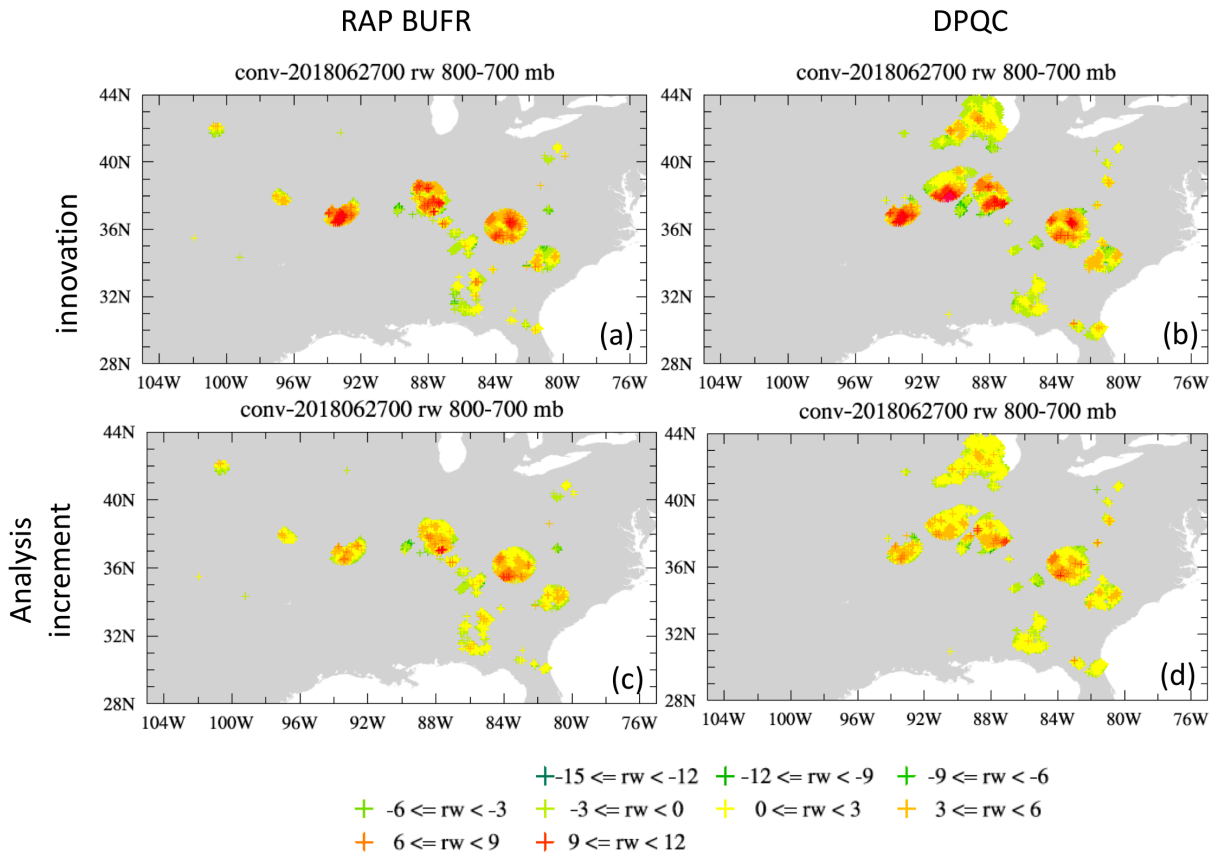

Figure 3.7, Radial velocity innovation (O-B, upper row) and O-A (lower row) in radial velocity observation locations between the 800-700 mb levels from GSI analysis using the NCEP BUFR radial velocity file (left column) and the DPQC radial velocity file generated by DTC (right column). The GSI analysis uses the modified RW operator with VADQC turned off.

Figure 3.7 compares the innovation of the radial velocity in GSI analysis with NCEP BUFR file (Fig. 3.7a) and with DPQC RW data (Fig. 3.7b). The biggest difference is that the DPQC RW includes more radar stations than NCEP BUFR. The reason for those radar stations missing in the NCEP BUFR file could be slow transferring of data during an active convective day, the short cutoff time in generating the BUFR file to meet rapid cycles, and the strict quality control for the radial velocity observations for operational application of the data. One main purpose of this test is to try using all available radial velocity observations to evaluate the impact of radial velocity on the HRRR storm forecast in the best available data scenario. Our radial velocity impact study from last year shows the NCEP BUFR radial velocity file did miss some radar stations and had strict quality control, which tossed many observations that could help with the analysis. The DPQC radial velocity observations are from NSSL with minimum quality control imposed. So, the DPQC RW consists of all possibly available radial velocity observations that GSI can use in real-time. After dealiasing, we applied DPQC data in GSI and did find more radar

stations. For some stations existing in both data sources, we have found that DPQC did include more observations in most of the cases (Fig. 3.7a and b).

The O-A from both data sources tells the same story as the innovation fields. The DPQC clearly includes new stations and more observations for most of the stations existing in BUFR file (Fig. 3.7c and d). When comparing the innovations and O-A fields for GSI analysis with DPQC radial velocity (Figure 3.7b and d), we can see the O-A are smaller than the innovations. This verifies that the DPQC data did get used by the GSI to modify the wind background to fit closer to the radial velocity observations, which is how a data analysis system should behave when data are being used.

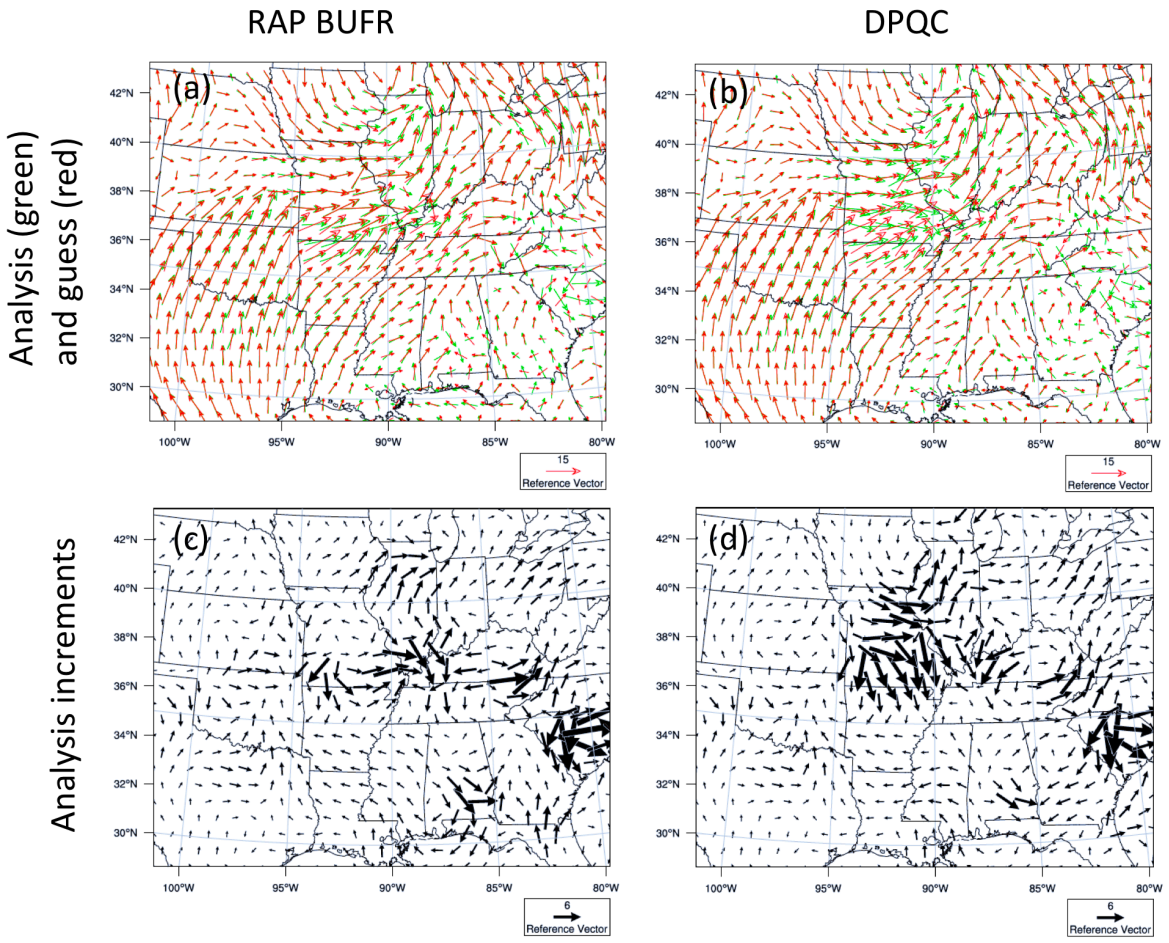

Figure 3.8, Background (red) and analyzed (green) wind vector (upper row) and wind analysis increments (lower row) at model level 7 from GSI analysis using the NCEP BUFR radial velocity file (left column) and the DPQC radial velocity file generated by DTC (right column). The GSI analysis uses modified RW operator with VADQC turned off.

Figure 3.8 gives the wind vector fields from the background and analysis (Fig. 3.8a and b). Even from full wind vector analysis field, we can see DPQC data clearly modified the wind fields in

the center of the analysis domain. The analysis increments (Fig 3.8c and d) also show that the DPQC data has a larger impact on the final analysis than the BUFR file, simply because the DPQC data includes more observations.

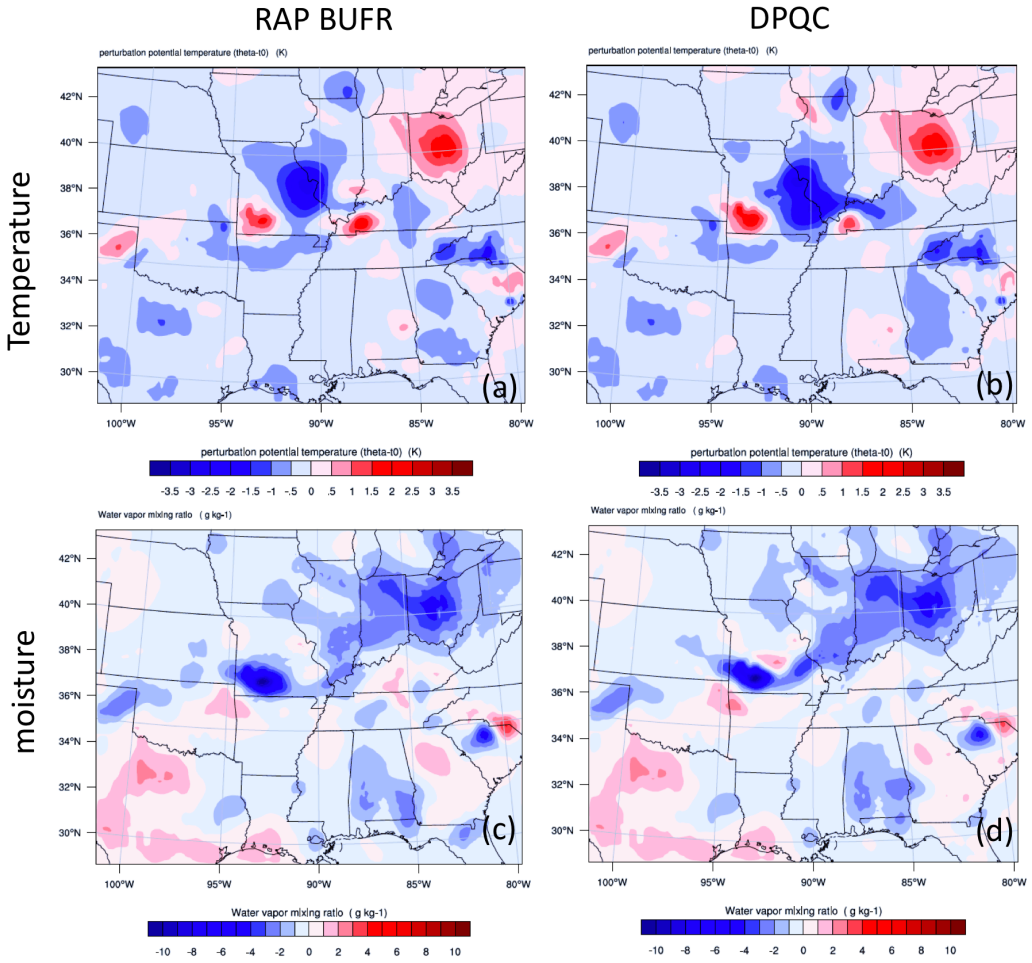

Figure 3.9, Analysis increment at model level 7 for temperature and moisture from GSI analysis using NCEP BUFR radial velocity file (left column) and DPQC radial velocity file generated by DTC (right column). The GSI analysis uses the modified RW operator with VADQC turned off.

Comparing the temperature and moisture analysis increment when using the two radial velocity data sources, we see that the overall patterns are very similar. But the analysis increments in the center of the analysis domain from DPQC clearly cover a larger area. The larger number of observations from DPQC does make some difference in analysis results, either directly on the wind vector fields or indirectly on the temperature and moisture field through wind-mass balance and the moisture analysis variable definition.

After those single case studies, we are confident that the DPQC data has been correctly processed and analyzed in GSI. We therefore move forward to run retrospective experiments to investigate the impact of the DPQC radial velocity data on the HRRR forecast.

4. Update and enhance HRRR on community HPC

In AOP 2017, we installed the HRRR operational system on Cheyenne to provide a HRRR functionally similar experiment system to the research community. The HRRR system built last year is HRRR version 3. Also, we used boundary condition and observation files preprocessed on JET to simplify the community HRRR system. The simplified HRRR on Cheyenne helped us focus on building the most important components of the system, such as GSI, WRF, and UPP. It also provides a testing environment very close to the one used by the GSD RAP/HRRR group. The control retrospective tests on Cheyenne and JET showed mostly identical results, which indicates we have built a HRRR functionally similar system on Cheyenne that can be accessed easily by the research community.

In this AOP, we updated the HRRR system to use GSI for HRRR version 4. We also added the HRRR components that generate initial and boundary conditions, and the whole suite of observation data preprocessing. The updated HRRR system will not depend on JET to provide the boundary condition and process observations. The entire HRRR system can be run on Cheyenne as long as RAP post-processed grib2 files and observation files are available. Because there are more than ten individual preprocess applications needed for HRRR to run, DTC helped GSD to develop a CMake compiling system that can make all the preprocess executables in one run, which greatly simplified the compiling of HRRR components.

5. June 24-30, 2018 retrospective experiments

After building the updated HRRR system on Cheyenne, we staged a week of observations and RAP forecast grib2 files from June 24 to 30, 2018 for HRRR to conduct retrospective experiments to evaluate the impact of DPQC radar radial velocity observations on the HRRR forecast.

5.1 Retrospective experiment period and setups

During June 24-30, 2018, a low-pressure system moved across the central and eastern US (Fig. 5.1c). It induced a period of active storms with tornadoes, high winds, and hail over central and eastern US CONUS (Fig 5.1a and b). There were also extensive strong precipitation events during the pass of the low-pressure system (Fig.5.1d). Most of the storms during this period occurred in relatively flat topographical areas covered by good conventional and radar observations. Hence we picked this period for our retrospective experiment to further study the impact of the DPQC radial velocity observations in a high-resolution rapidly updated cycling system such as HRRR. To reduce the computation cost, we generated a smaller 3-km resolution domain that covers the central and eastern US as our test domain (Fig 5.2). Except for domain size, all other configurations are closely following HRRR version 4.

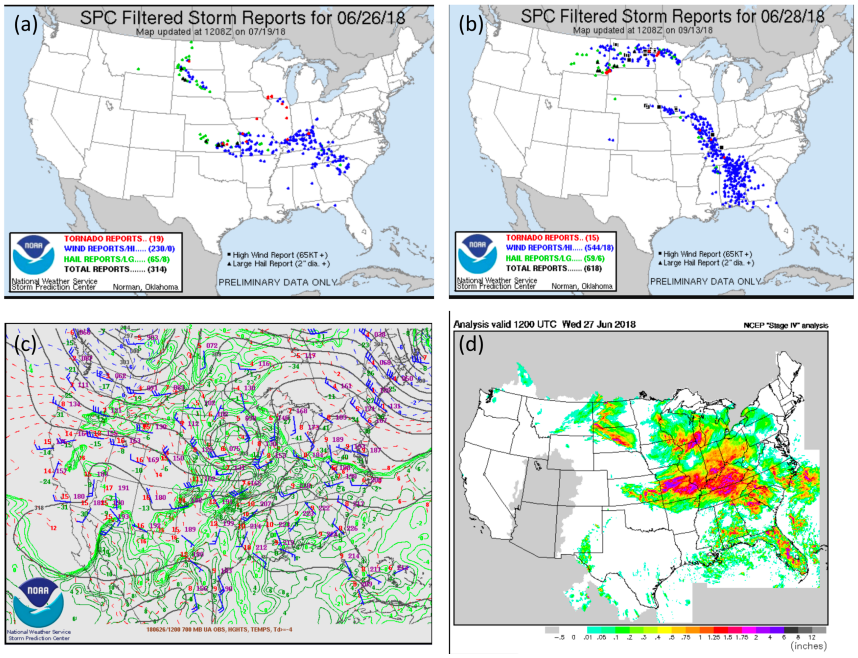

Figure 5.1, SPC storm reports for June 26 and 28, 2018. 700 mb weather map for height, wind, and temperature at 12Z on Jun 26, 2018 from SPC, and past 24-h accumulated precipitation (water equivalent inches) valid at 12Z, June 27, 2018 from NCEP "stage IV" analysis.

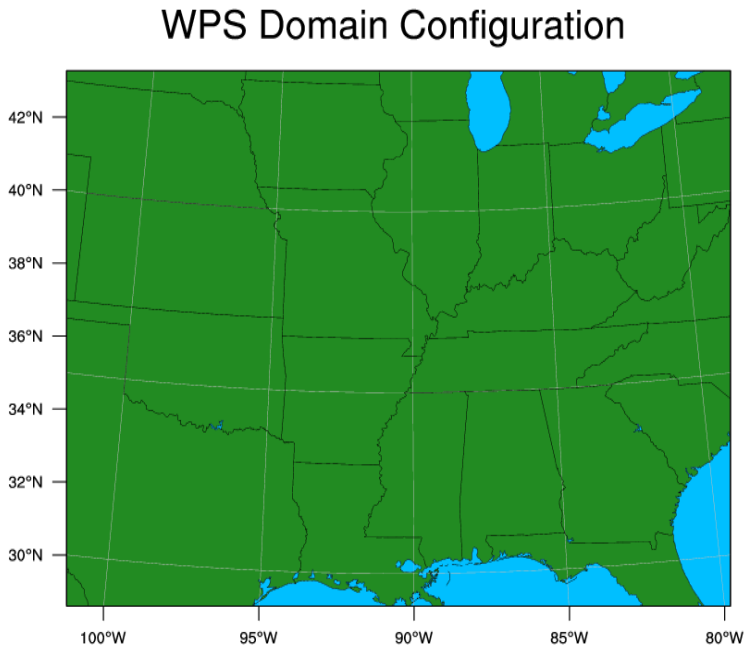

Figure 5.2, the retrospective experiment domain

The DPQC radial velocity observations from the radar stations located inside the experiment domain and the duration of the experiment were collected and processed through the "bufrizing" and dealiasing steps developed by DTC. The final DPQC observations are saved in hourly BUFR files with wind observation time from -30 to 30 minutes.

Four retrospective experiments, including a control and three experimental runs, were conducted to study the impact of GSI radial velocity observation operator, the VADQC, and the use of the new DPQC radial velocity observations on the HRRR forecast. The configurations of each retrospective experiment are shown in the table below.

Table 5.1, List of the retrospective experiments

Experiment name	Radial velocity observation resources	GSI radial velocity observation operator	VAD QC
control	NCEP BUFR RW file	Default	on
Exp 1	NCEP BUFR RW file	Modified	on
Exp 2	DPQC RW processed by DTC	Modified	off
Exp 3	DPQC RW processed by DTC	Modified	on

5.2 Experiment results

Radar radial velocity can provide detailed wind structure of small convection systems but assimilating that information into initial fields and therefore improving the storm forecast is very challenging. Through the three experiments, we will examine the impact of assimilating DPQC radar radial velocity on both the environmental forecast and the storm system itself in HRRR.

5.2.1 impact on the environment forecast

The full picture of the impact of assimilating radar radial velocity on the environmental forecast of HRRR can be seen with scorecards that include major upper air and surface variables. How to interpret the scorecard is illustrated in Fig. 5.3. Red boxes and triangles indicate improvements of the experiment over control run, which we are looking for, while green means degradation of the forecast skill when test targets of certain experiments are applied.

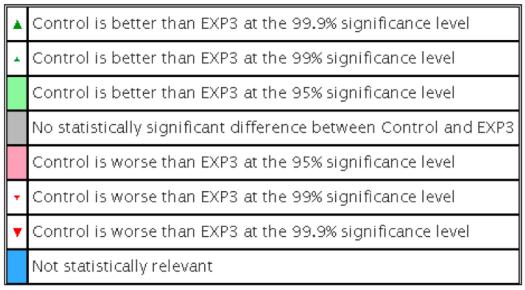

Figure 5.3 Interpretation of scorecard

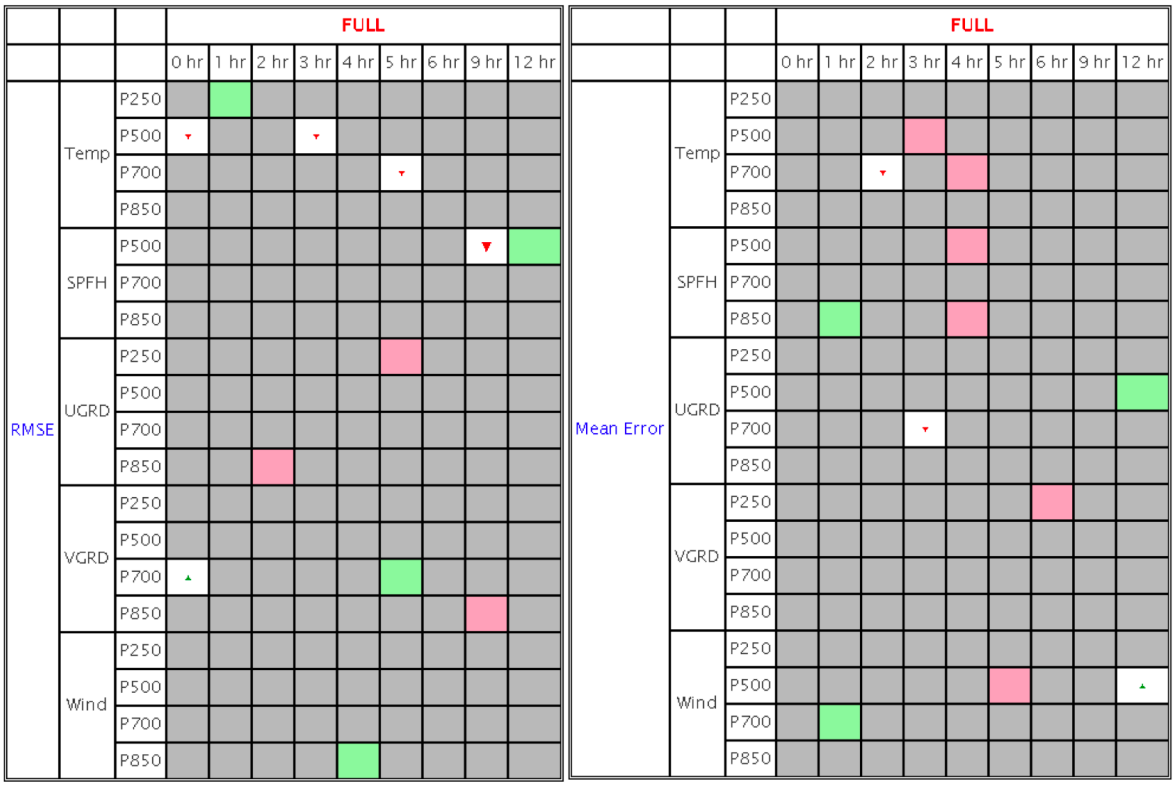

Figure 5.4, upper air scorecard for control and EXP1.

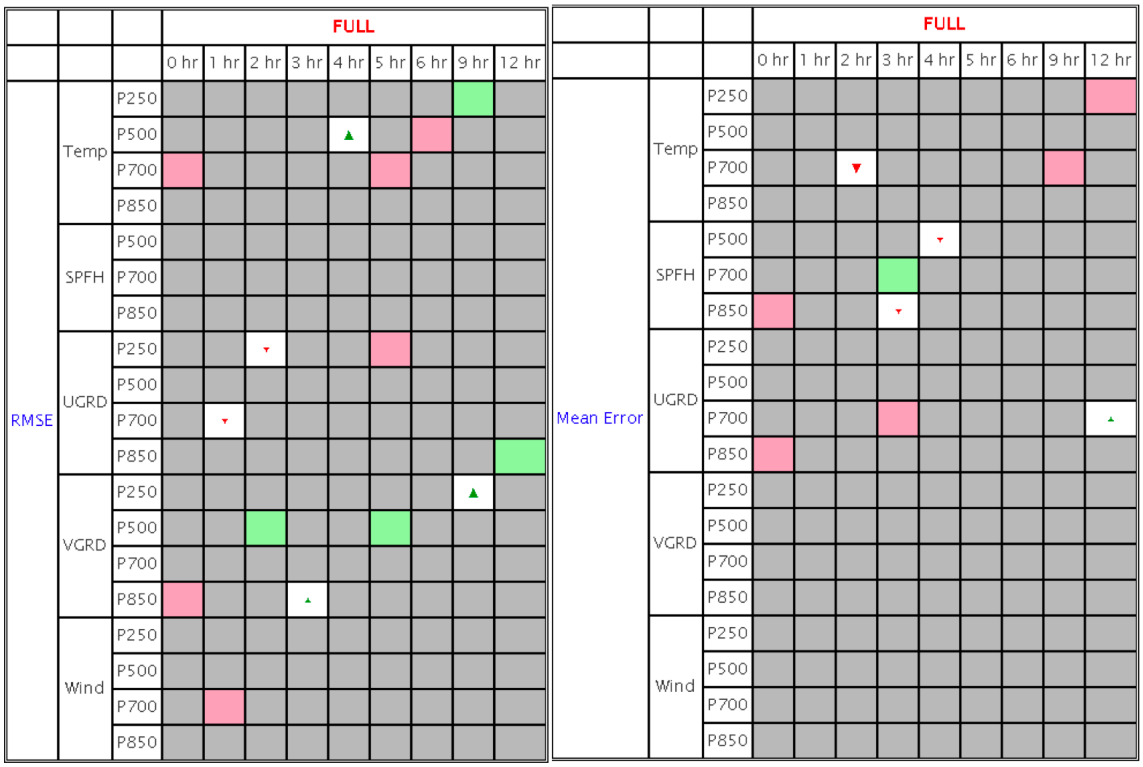

Figure 5.5, upper air scorecard for control and EXP2.

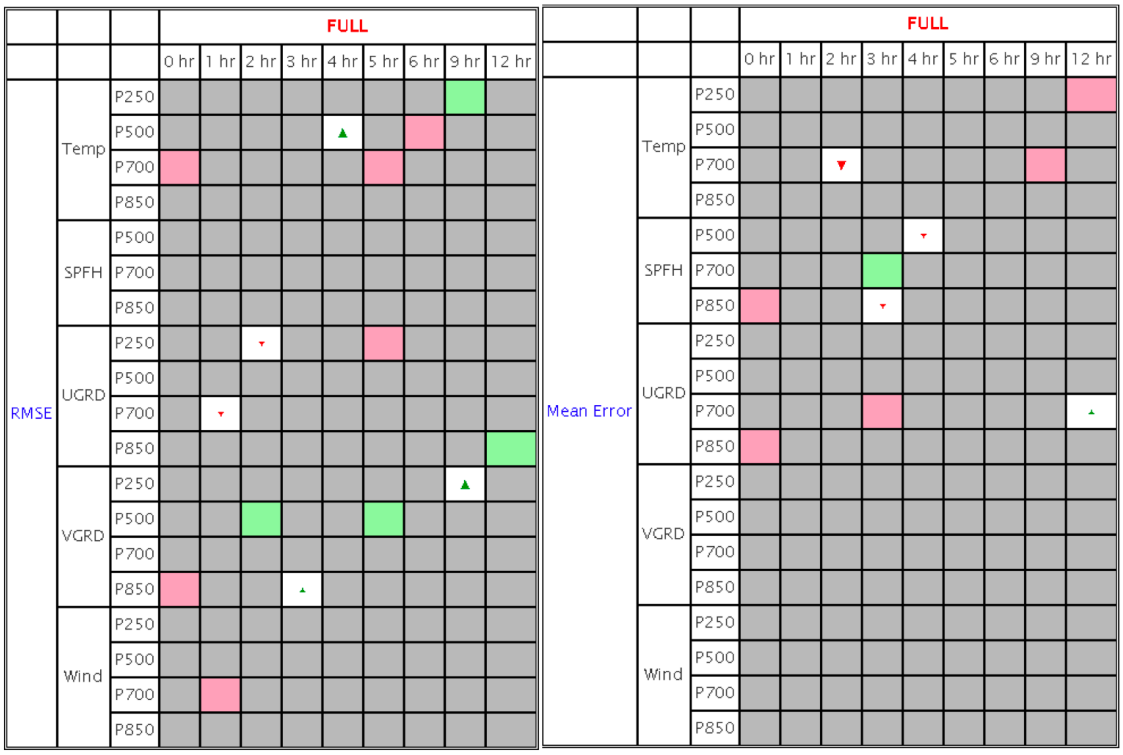

Figure 5.6, upper air scorecard for control and EXP3.

Figures 5.4, 5.5, and 5.6 show the upper air scorecards comparing the control experiment to experimental runs EXP1, EXP2, and EXP3. We can see that the majority of verification variables are neutral. Figure 5.7 gives the vertical profiles of the relative humidity RMSE and bias, as an example to show the neutral impact from the experimental runs. In DTC AOP 2017 T&E task, we tested a set of the configurations related to the radial velocity assimilation and found the neutral impact from assimilating radial velocity on both upper and surface environmental fields in the HRRR forecast. From those upper air verification matrices, we can conclude that applying radial velocity has little impact on the upper air environmental forecast. This is also consistent with the results on radial velocity impact from operational experiments.

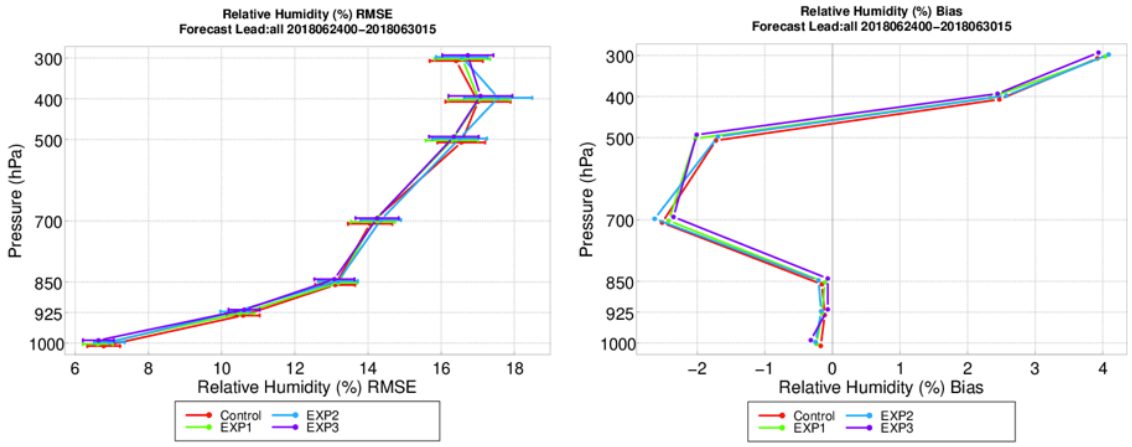

Figure 5.7, Vertical profiles of the relative humidity RMSE (left) and Bias (right) from the control run (red) and the three experimental runs.

The scorecards for the surface (Fig. 5.8) show a different story from AOP 2017 and from the upper air statistics. The scorecard mostly shows red boxes and triangles, which indicate that assimilating radial velocity improved the forecast of certain surface fields. The experiment EXP1 used the modified observation operator and these results illustrate it can improve the short-term forecast (within 2-h of forecast) for the surface moisture field. Experiment 3 actually showed less impact, because the use of VADQC tossed out most of the observations from the DPQC radial velocity data source. The experiment EXP2 is the focus of our test, because it used the modified observation operator, DPQC radial velocity observations, and turned VADQC off. The impact of those changes is clear on the surface forecast. The surface wind and moisture showed clear improvements up to 6-h forecast.

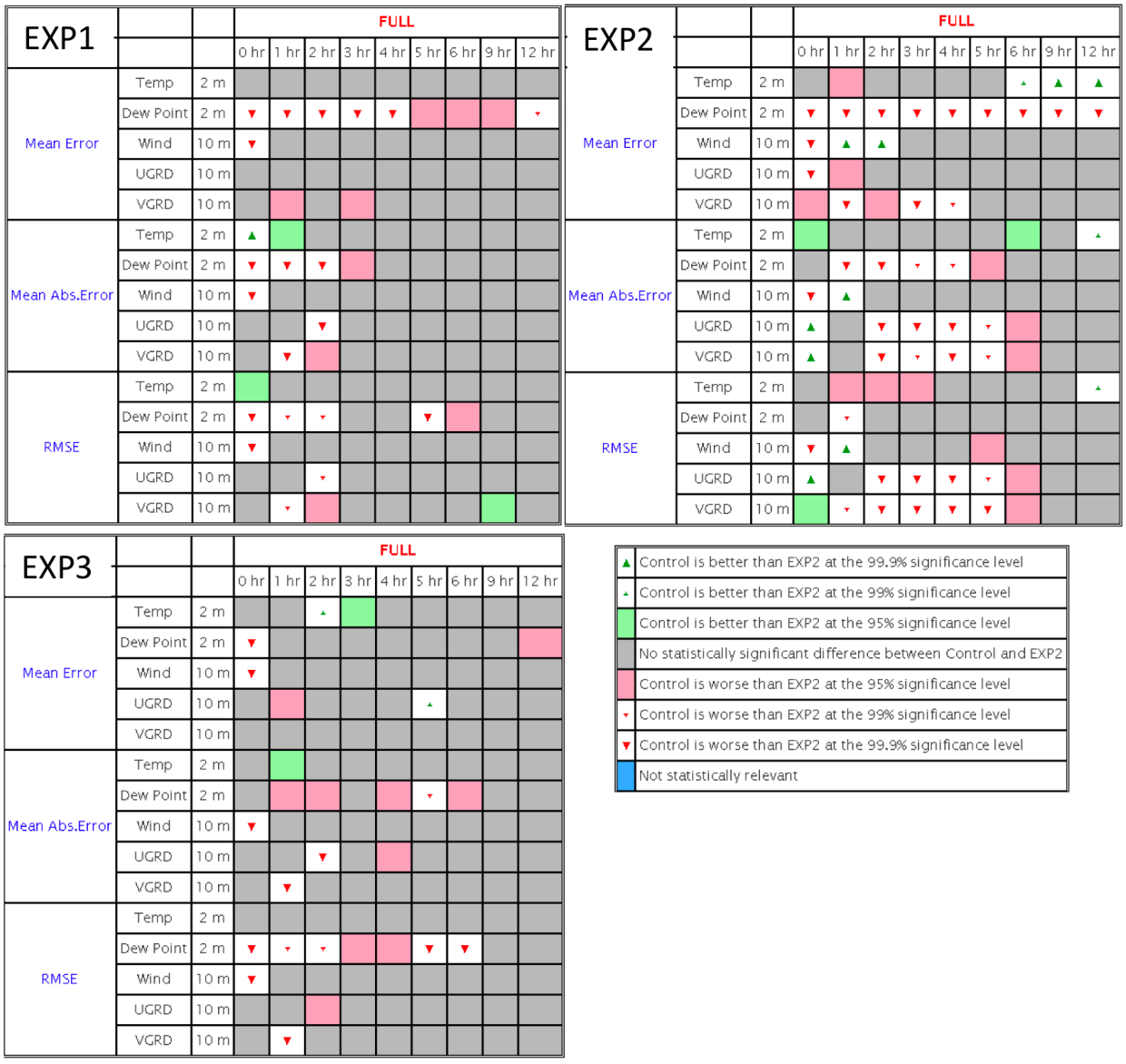

Figure 5.8, surface scorecard for control and experiments EXP1, EXP2, and EXP3.

Figures 5.9 to 5.12 show the RMSE and bias of 2-m dew point temperature, 2-m temperature, and 10-m U and V wind in the first 12-h forecast against surface METAR observations for four runs and the difference of EXP1, EXP2, and EXP3 against the control run. These figures tell the same story as the scorecard but include more details. Most of the RMSE and bias values from those four experiments are close to each other or mixed. But dew point temperature bias for the first 12-h forecast and U and V wind RMSE in the first 6-hour forecast do show some improvement for EXP2, which used DPQC radial velocity with modified observation operator and VADQC turned off. EXP2 has the largest amount of observations used in the analysis because of the new data source and no VADQC, as well as the observation operator that can maximize the use of the observations.

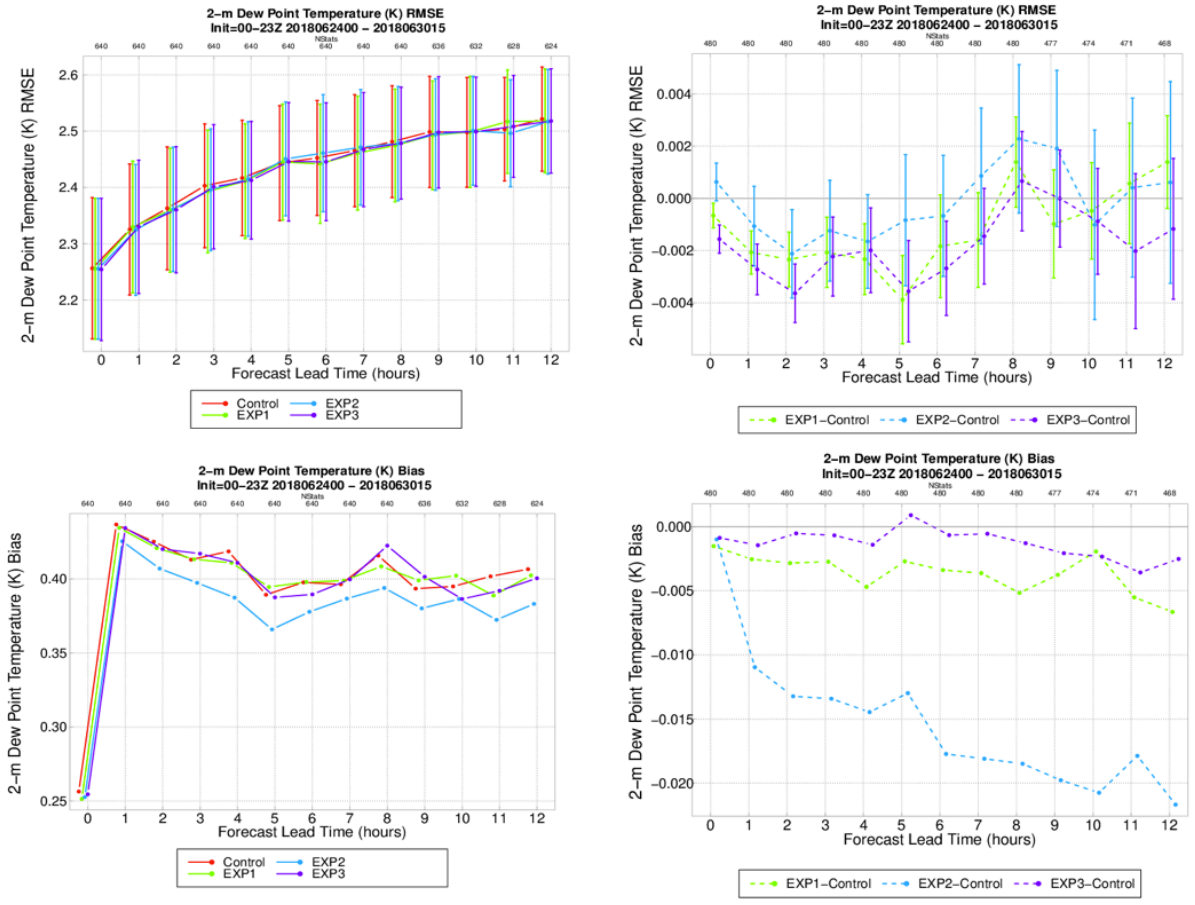

Figure 5.9, RMSE and bias of 2-m dew-point temperature in the first 12-h forecast against surface METAR observations for four experiments: control, EXP1, EXP2, EXP3 (left column) and the difference of EXP1, EXP2, EXP3 against control (right column).

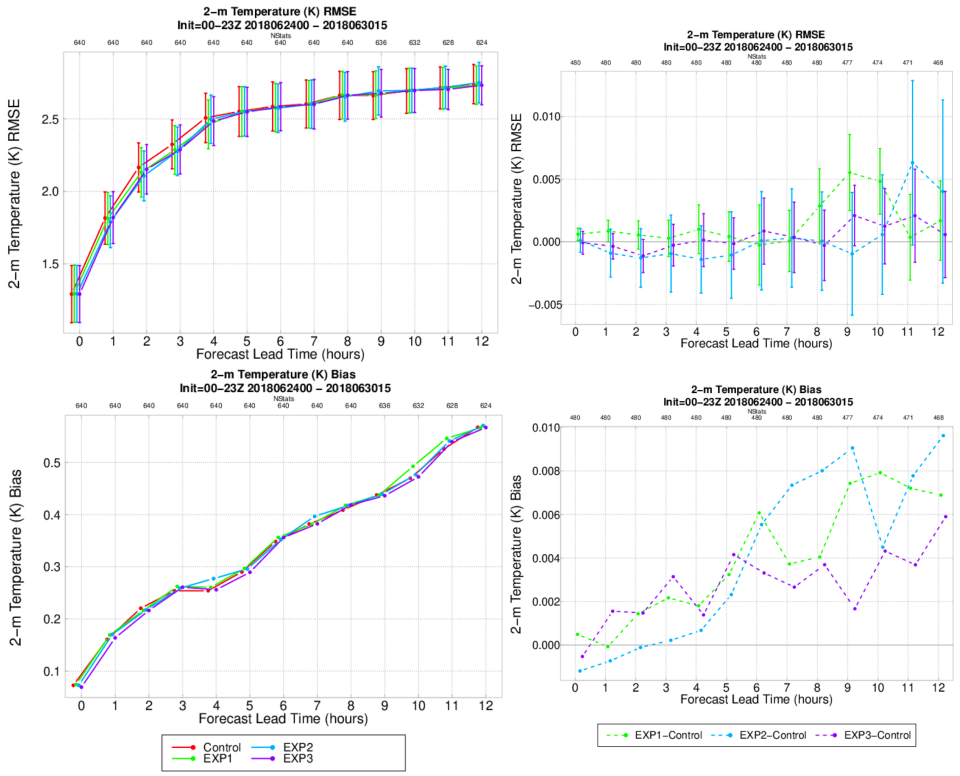

Figure 5.10, same as Figure 5.9 but for 2-m temperature.

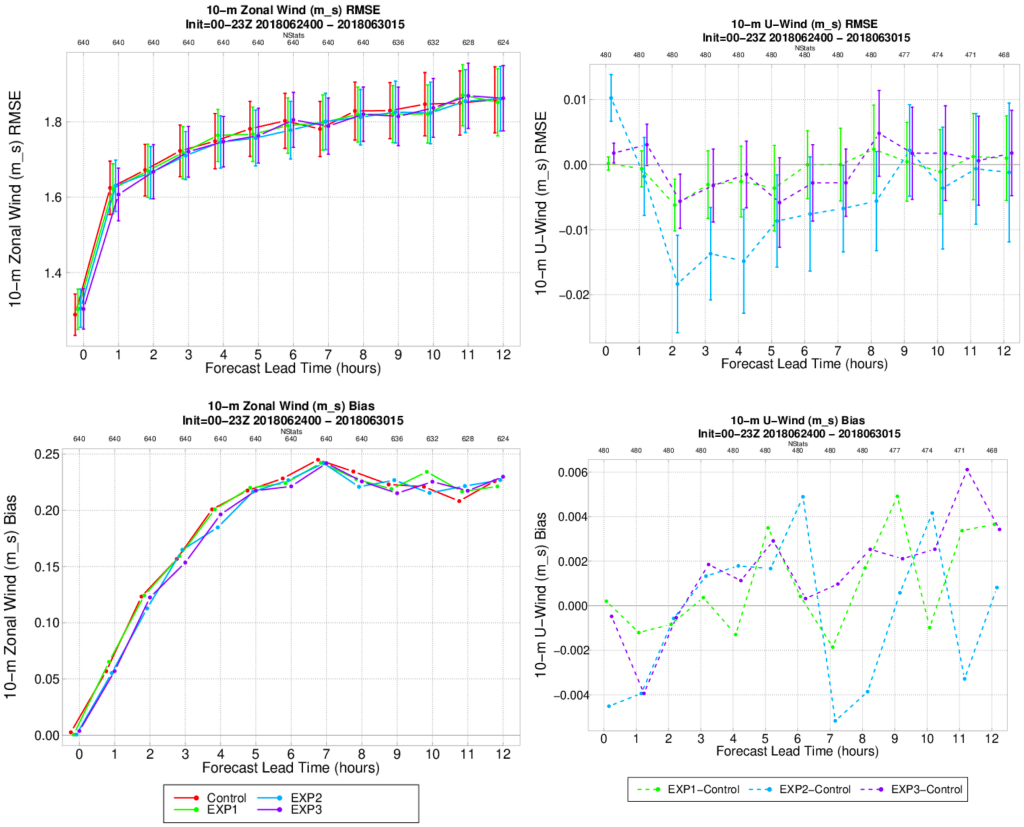

Figure 5.11, same as Figure 5.9 but for 10-m zonal wind.

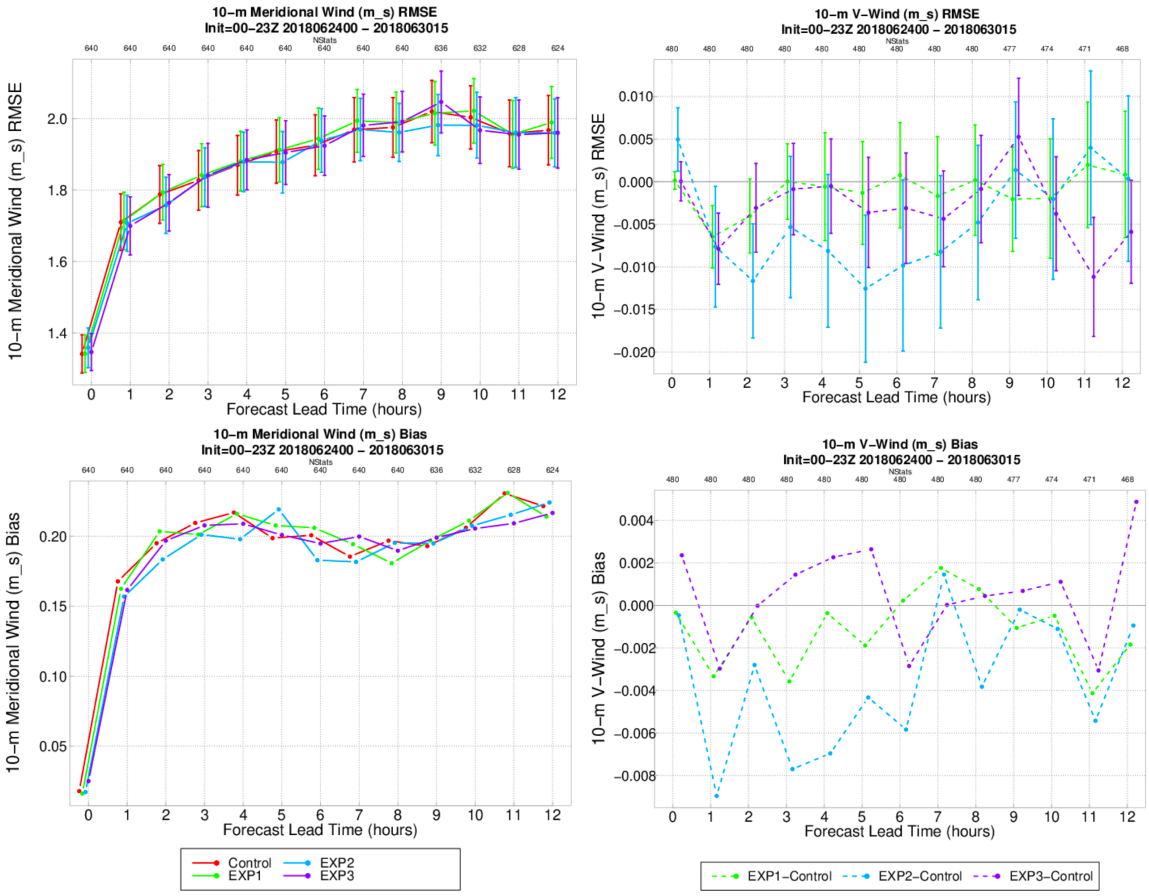

Figure 5.12, same as Figure 5.9 but for 10-m meridional wind.

5.2.2 Impact on the reflectivity forecast

In this section, we will show several verification statistics using reflectivity to examine the impact of assimilating radar radial velocity on the storm forecast in HRRR.

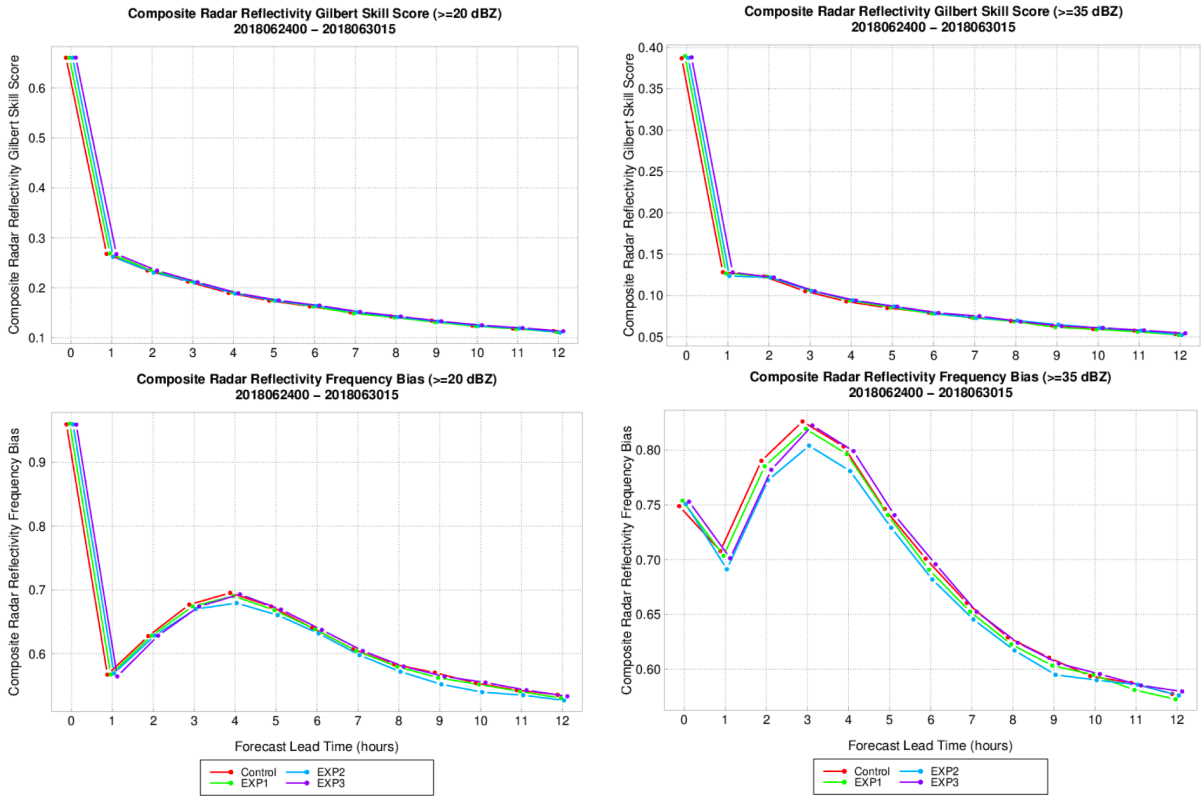

Figure 5.13, Gilbert Skill Score (upper row) and frequency bias (lower row) for 0 to 12-h forecast composite reflectivity greater than or equal to 20 dBZ (left column) and 35 dBZ (right column).

Figure 5.13 shows the Gilbert Skill Score (GSS) and frequency bias for 0 to 12-h forecast of composite reflectivity greater than or equal to 20 dBZ and 35 dBZ. We can see that the GSS for all four experiments are very close to each other. The frequency bias for composite reflectivity greater than or equal to 20 dBZ for all four experiments are also very close to each other. The only difference among those experiments is the frequency bias for composite reflectivity greater than or equal to 35 dBZ. EXP2 has somewhat lessfrequency bias than those from other three experiments for the 2-h to 5-h forecast. Because the radial velocity mainly relates to small-scale wind field structure, the analysis of radial velocity in general cannot change the environment for storm development. The very close GSS and frequency bias values from these experiments indicate that assimilating radial velocity cannot change storm distribution and strength in a whole domain and long-term sense.

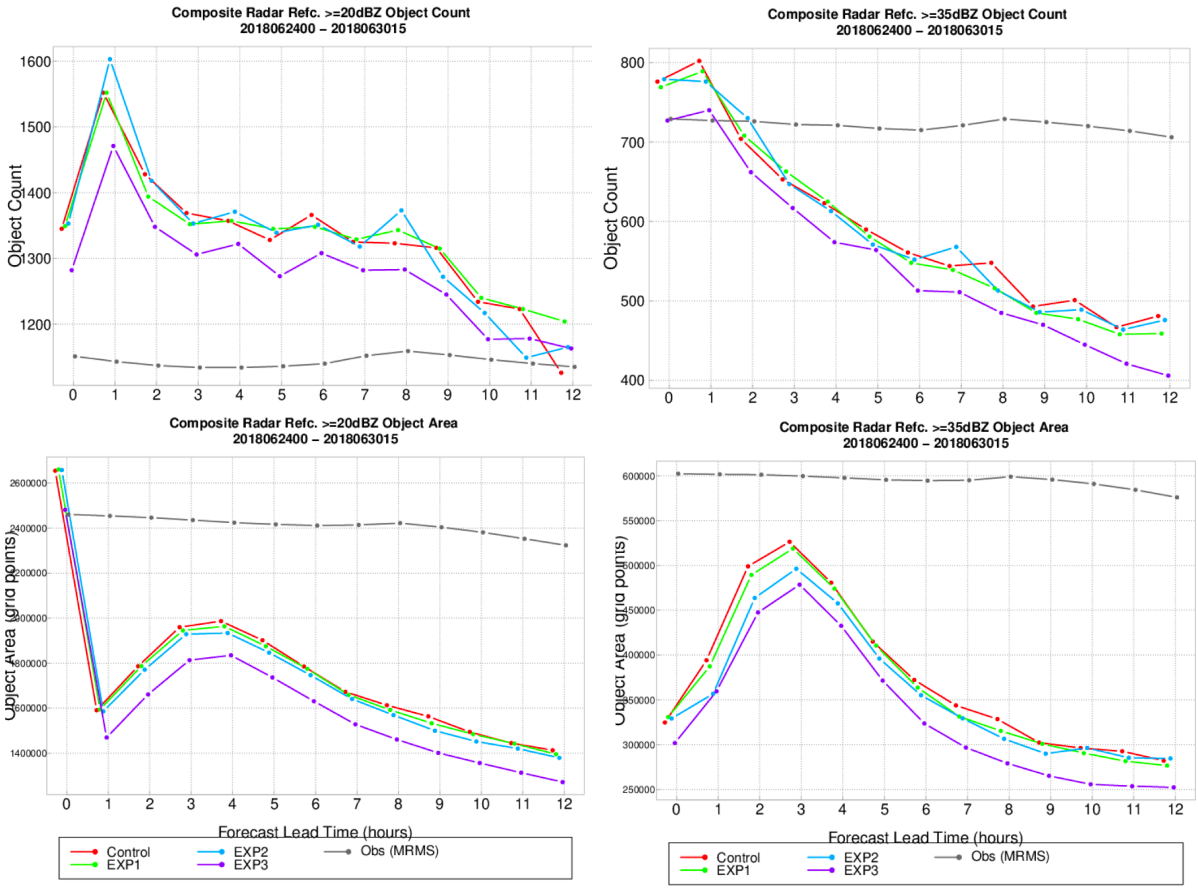

Figure 5.14, Object count (upper row) and object area (low row) of 0 to 12-h forecast and observed composite reflectivity greater than or equal to 20 dBZ (left column) and 35 dBZ (right column).

To check more details of the storm forecast, Method for Object-Based Diagnostic Evaluation (MODE) statistics were calculated for those four experiments. The object counts for >=20 dBZ and >=35 dBZ composite reflectivity (Fig 5.14, upper row) has a clear pattern that starts with a higher number of cells meeting the threshold compared to the observed cells but the pattern decreases rapidly with the forecast length. The >=20dBZ composite reflectivity has higher than observed counts but the >=35dBZ composite reflectivity (strong storms) has far less counts than the observed in the forecast longer than 3-h. The corresponding object areas for both >=20 dBZ and >=35 dBZ (Fig. 5.14, lower row) show far fewer object areas than the observed ones. Those statistics indicate the storm forecast in HRRR tends to have many smaller sized cells compared to the observed reflectivity field, especially for weaker storms (>=20 dBZ).

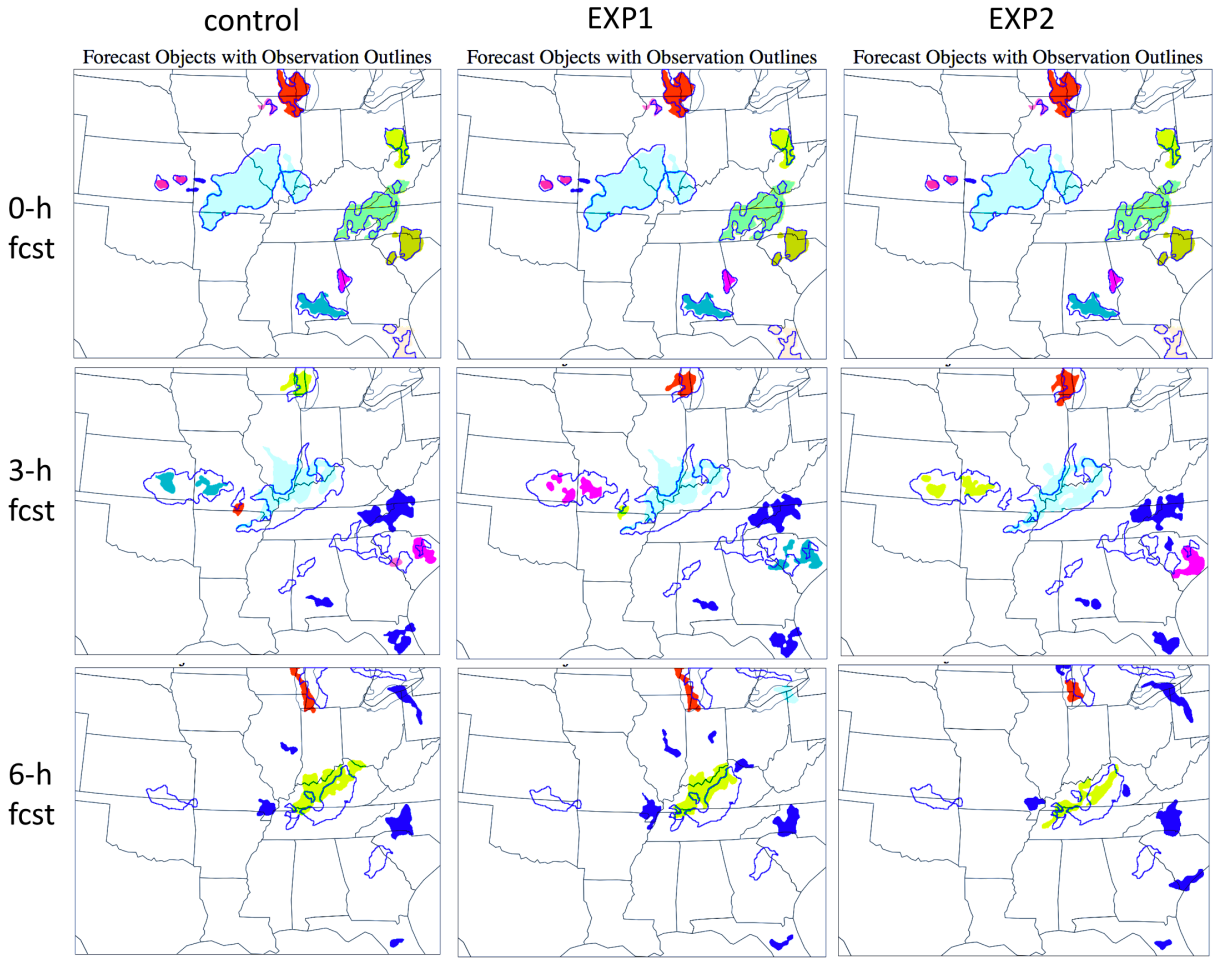

Figure 5.15, Forecast objects (colored area) with observation outlines of reflectivity greater than or equal to 20 dBZ for 0-h (upper row), 3-h (middle row), and 6-h (low row) forecast from 00Z, June 27, 2018 in experiments control (left column), EXP1 (middle column), and EXP2 (right column).

Figure 5.15 gives an example of object distributions from MODE verification at 0-h, 3-h, and 6-h forecast time. At the initial time, observed objects generally match the forecast ones well, except that the initial field missed several observed cells. The forecast objects become much smaller in size after three hours and are further reduced (or disappear) at the 6-h forecast. Another interesting characteristic is that the objects in control and EXP1 are very close to each other but the objects in EXP2 shows a bigger difference from control and EXP1, which indicate the impact of the DPQC radial velocity observations and with the VADQC turned off. With the larger number of radial velocity observations used in the analysis like EXP2, it is possible to change the behavior of the storm cells but not the larger scale distribution pattern of the storms.

The GSS and frequency bias (Fig. 5.13), and the object counts and areas from MODE verification, (Fig. 5.14) showed the similar characteristics of the storm forecasts. The use of radial velocity doesn't impact the overall statistics of the HRRR forecast in environment and big storm structure and propagation. But, the use of radial velocity could make some difference in

the forecast for the single cells or in some detailed features in storm system. We checked the composite reflectivity from 0-h, 3-h, and 6-h forecast for one cycle in control, EXP1, and EXP2, and compared them to the observations (Fig. 5.16) to see if there was any change in an individual storm from the use of the radial velocity.

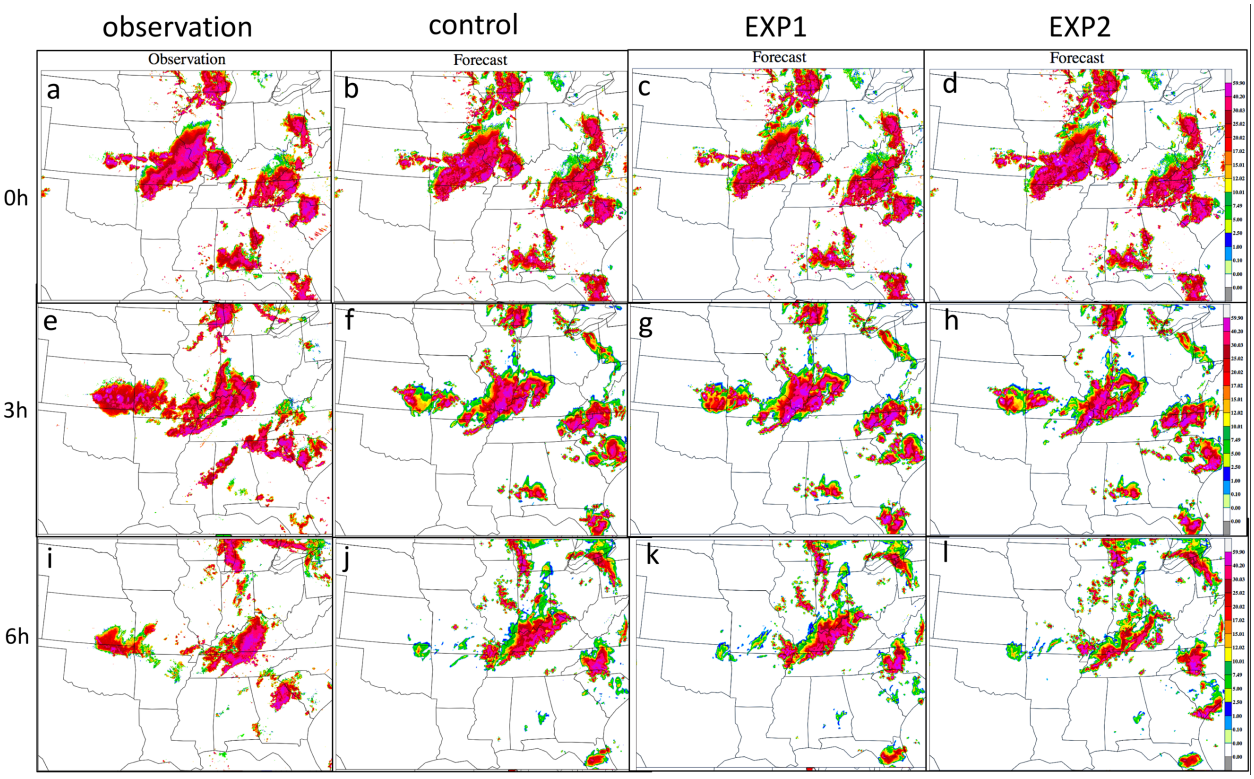

Figure 5.16, Composite reflectivity for 0-h (upper row), 3-h (middle row), and 6-h (low row) forecast from 00Z, June 27, 2018 in experiments control, EXP1, and EXP2, with corresponding observed composite reflectivity at forecast valid time.

The composite reflectivity from the initial fields of control, EXP1, and EXP2 (Fig 5.16b-d) are very close to the observed values. This is due to the application of the GSD non-variational cloud analysis in GSI that uses observed reflectivity to adjust precipitable hydrometeor fields. After a 3-hour forecast, the difference between experiments and the observation showed up. In general, the 3-h forecast from three experiments captured major storm systems around lake Michigan, northwest of Kentucky, over South Carolina, and east of Kansas—very well in location and strength, but they all over-forecasted storms in east Pennsylvania, north Florida, and south Alabama, and missed storms in north Mississippi (Fig. 5.16e-h).

The 3-h forecast composite reflectivity from the control and EXP1 (Fig 5.16f and g) are very close to each other, but we still can find some subtle differences between them. For example, the storm systems in east Kansas and west Mississippi—the similarity of the two forecasts and the subtle difference shows that the modified observation operator can impact the results on some level but that the impact is limited. When adding the composite reflectivity from the EXP2 3-h forecast (Fig 5.16h), the difference between EXP2 and the other two experiments becomes

larger. Even though the general pattern, distribution, and strength of the storm systems are quite similar, we do find subtle differences in many of the storm systems, such as the sharper front line for the storms in northeast Kentucky. The increased difference from EXP2 is encouraging. With proper quality-controlled observations and the improved observation operator, radial velocity can impact the storm forecast and change the storm structure. This opens the door to further investigation and possible improvements in applying radial velocity in HRRR and other storm modeling systems.

The 6-h forecast from the three experiment give a good forecast to the storms in Kentucky and Tennessee, and the storms in Lake Michigan, but either missed or over-forecasted other storms. The experiments control and EXP1 are very close to each other and EXP2 shows more difference from other two experiments because of using DPQC radial velocity and turning off the VADQC in GSI analysis.

6. Summary

In AOP 2018, the DTC data assimilation team continued to use the HRRR operational version on NCAR HPC to study the impact of assimilating radar radial velocity on storm forecasts. Radar radial velocity can provide many details of wind structure related to convection. But, the use of radial velocity for improving operational convective forecast with high resolution storm-scale modeling is very challenging.

The radial velocity observations for AOP 2018 testing are dual-polarized quality controlled (DPQC) radar radial velocity data from NSSL. We used this data resource because one of the findings in our AOP 2017 tests was that the NCEP operational BUFR radial velocity file for RAP/HRRR has gone through a very strict quality control process and many observations have been tossed out because of this strict quality control process. The DPQC radial velocity data has only gone through basic quality control and has kept a significant amount of raw radial velocity observations. DTC developed new scripts to convert the original DPQC observations from single tilt NetCDF files to an hourly BUFR file including all volume and radar stations within a certain time window and domain. Then another new code developed by DTC applied three dealiasing steps (global, local, and VAD) to those BUFR files to correct folded radial velocity. The processed DPQC observations used in the retrospective experiments produce reasonable results and we think these new “bufrizing” and dealiasing tools can be used in the real-time or operational system for assimilating DPQC radial velocity.

To better understand the impact of the new DPQC radial velocity observations, we conducted a series of single case GSI runs to compare the analysis increments of using the NCEP BUFR radial velocity file and the DPQC radial velocity. We found that the current radial velocity observation operator was not designed for convection scale analysis. In order to use more observational information from radial velocity, we modified the GSI radial velocity observation operator to directly use the radial velocity calculated from nearby grid points as the background to calculate the innovations. Another finding from the single case study is that applying VAD quality control

in GSI radial velocity data will toss out the majority of the observations, especially for DPQC radial velocity data (because some DPQC radar stations have no corresponding VAD observations). By using the modified observation operator and turning off the VAD QC, the impact of the radial velocity from both the NCEP BUFR radial velocity file and the DPQC radial velocity data on the analysis was significantly improved. In this study, we did find that the DPQC radial velocity data resource was able to provide more observations than the NCEP BUFR radial velocity file, which is the operational feed to current RAP and HRRR operations.

After updating the HRRR system on community HPC, four week-long retrospective experiments from June 24 to 30, 2018 were conducted to study the impact of the DPQC radial velocity, the modified radial velocity observation operator, and VADQC on HRRR forecast. The control experiment used the current HRRR configuration and operator for radial velocity assimilation. Experiment 1 was to study the impact of the modified radial velocity operator. The modified observation operator can get more radial velocity observations that have small innovations used in the analysis. It produced similar results as the current operator in term of the environment forecast, but the modified operator did change some storm structure in the forecast.

Experiments 2 and 3 used DPQC radial velocity observations but most of the DPQC observations in experiment 3 were tossed out because of the VADQC. So, experiment 3 looks very close to the control experiment. Experiment 2 used the modified radial velocity operator with VADQC turned off. The configuration of experiment 2 maximized the impact of the radial velocity observations and it did show clear impacts on the surface forecast and storm forecast in HRRR. The slight improvement of the surface moisture and wind forecast in experiment 2 over the control experiment is encouraging, because in most of our experiments adding the radial velocity observations can only produce a neutral impact. The changes of the storm forecast in experiment 2 over the control experiment also verified the increased impact of radial velocity on storm forecasts. Those results indicate the that radial velocity, after proper quality control and used through a suitable observation operator, can contribute to the storm forecast.

Through the AOP 2017 and 2018 study of radial velocity assimilation with HRRR, we gained a much deeper understanding of the radial velocity data feed, quality control process, observation operator, and possible contributions to the storm forecast. The outcome regarding the radial velocity data process and assimilation methods gained in this study will certainly help in building the FV3-based high resolution data assimilation system because it will use GSI and share most of the data and code with the current HRRR system.